

SIRT7 couples light-driven body temperature cues to hepatic circadian phase coherence and gluconeogenesis

Zuojun Liu^{1,2,3,9}, Minxian Qian^{1,2,3,9}, Xiaolong Tang^{1,2,3}, Wenjing Hu^{2,4}, Shimin Sun^{2,4}, Guo Li⁵, Shuju Zhang^{2,3}, Fanbiao Meng^{2,3}, Xinyue Cao^{2,3}, Jie Sun^{1,2,3}, Cheng Xu^{1,2,3}, Bing Tan^{1,2,3}, Qiuxiang Pang⁴, Bosheng Zhao⁴, Zimei Wang^{1,3}, Youfei Guan⁶, Xiongzhong Ruan^{7,8}, Baohua Liu^{1,2,3*}

¹Guangdong Key Laboratory of Genome Stability and Human Disease Prevention, Shenzhen University Health Science Center, Shenzhen, China.

²National Engineering Research Center for Biotechnology (Shenzhen), Carson International Cancer Center, Medical Research Center, Shenzhen University Health Science Center, Shenzhen, China

³Department of Biochemistry and Molecular Biology, School of Basic Medical Sciences, Shenzhen University Health Science Center, Shenzhen, China.

⁴Anti-aging & Regenerative Medicine Research Institution, School of Life Sciences, Shandong University of Technology, Zibo 255049, China

⁵Department of Dermatology, Xiangya Hospital, Central South University, Changsha, China.

⁶Advanced Institute for Medical Sciences, Dalian Medical University, Dalian 116044, China.

⁷Department of Renal Medicine, University College London, London, UK.

⁸Centre for Lipid Research and Key Laboratory of Molecular Biology for Infectious Diseases (Ministry of Education), Institute for Viral Hepatitis, Department of Infectious Diseases, The Second Affiliated Hospital, Chongqing Medical University, Chongqing, China.

⁹These authors contributed equally to this work.

*Correspondence should be addressed to Dr Baohua Liu (ppliew@szu.edu.cn)

Abstract

The central pacemaker in the hypothalamic suprachiasmatic nucleus (SCN) synchronizes peripheral oscillators to coordinate physiological and behavioral activities throughout the body. How circadian phase coherence between the SCN and the periphery is controlled, is not well understood. Here, we identify hepatic SIRT7 as an early element responsive to light that ensures circadian phase coherence in the murine liver. The SCN-driven body temperature (BT) oscillation induces rhythmic expression of HSP70, which promotes SIRT7 ubiquitination and proteasomal degradation. Acute temperature challenge dampens the BT oscillation and causes an advanced liver circadian phase. Further, hepatic SIRT7 deacetylates CRY1, promotes its FBXL3-mediated degradation and regulates hepatic clock and glucose homeostasis. Loss of *Sirt7* in mice leads to an advanced liver circadian phase and rapid entrainment of hepatic clock upon daytime-restricted feeding. These data identify a novel BT/HSP70-SIRT7-CRY1 axis that couples murine hepatic clock to the central pacemaker and ensures circadian phase coherence and glucose homeostasis.

Keywords: Circadian clock, body temperature, SIRT7, CRY1, glucose homeostasis

Introduction

Physiological and behavioral activities are coordinated by an endogenous biological clock that is synchronized by a central pacemaker in the SCN^{1,2}. At the molecular level, circadian rhythms are sustained by an auto-regulatory transcriptional/translational feedback loop (TTFL), in which CLOCK and BMAL1 heterodimerize to promote *Cryptochrome* (*Cry1/2*) and *Period* (*Per1/2*) transcription; accumulating CRY and PER proteins dimerize and translocate to the nucleus, where they repress the transcriptional activity of the CLOCK:BMAL1 complex³⁻⁹. The CLOCK:BMAL1 complex also activates *Rev-Erba/β* and retinoic acid receptor-related orphan receptor (*Ror*) transcription; in turn, ROR stimulates while REV-ERBα/β suppresses *Bmal1* transcription via ROR elements (RORE)¹⁰⁻¹².

The endogenous biological clock is entrained by a variety of environmental signals, known as *Zeitgebers*. Light is a predominant *Zeitgeber* that entrains the central clock in the SCN via the retino-hypothalamic tract; the SCN then synchronizes subsidiary oscillators in the periphery¹³. Although still unclear at the molecular level, increasing evidence suggests that the synchronization is mediated by systemic cues, such as feeding activity, body temperature (BT) and hormones¹⁴. In mice, BT declines in the light, resting phase, but increases in the dark, active phase^{15,16}; the daily variation in BT integrates the central clock to hepatic clock via Heat shock factor (HSF1)-mediated stress response¹⁷⁻¹⁹. Light/dark (LD) cycle also regulates food intake behavior, thus coupling the central clock to metabolic processes²⁰⁻²². Of note, feeding serves as an independent *Zeitgeber* of the hepatic clock but not the central clock^{13,14}.

NAD⁺-dependent sirtuins are crucial nutrient sensors that couple metabolism to peripheral clocks. SIRT1 rhythmically deacetylates BMAL1 and histone H3 at circadian promoters to regulate the expression of clock-controlled genes (CCGs)²³. SIRT1 also deacetylates and thus destabilizes PER2 to modulate circadian clocks²⁴. SIRT6 instead, regulates the expression of CCGs rather than core TTFL elements in the liver²⁵. SIRT7 localizes in the nucleolus where it deacetylates H3K18 and desuccinylates H3K122 to modulate chromatin remodeling, gene transcription and DNA repair^{26,27}. While loss of *Sirt7* causes genomic instability and accelerated aging in mice²⁸, a biological function for SIRT7 in circadian rhythms is unclear.

All environmental *Zeitgebers*, and central and peripheral oscillators must be finely

aligned to ensure circadian phase coherence and avoid disrupted rhythmicity, which might lead to metabolic diseases and/or accelerated aging. For example, constant light exposure alters feeding activity and causes obesity in mice²⁰. Ablating the *Clock* gene disrupts feeding rhythms and metabolism and accelerates aging in mice^{29,30}. *Bmal1* knockout mice are arrhythmic and short lived^{7,31}. Intriguingly, only marginal effects were observed on *Per* and *Cry* rhythmicity in the liver when *Bmal1* expression was attenuated^{32,33}. Restricted feeding (RF) entrains the hepatic clock more rapidly in mice when the SCN is ablated³⁴. These suggest that the synchronizing cues from the central pacemaker counteract the phase entrainment of liver clock induced by RF, likely via a *Bmal1*-independent, yet unknown mechanism.

Here we present SIRT7 as an early responsive element to light-driven timing cues in the mouse liver. We found that BT oscillations induce rhythmic *Hsp70* transcription, and HSP70 interacts with SIRT7 to promote its ubiquitination and proteasomal degradation. SIRT7 deacetylates CRY1 and promotes its degradation mediated by FBXL3, coupling the hepatic clock to the central pacemaker. Hepatic SIRT7 thus regulates circadian glucose homeostasis and hepatic gluconeogenesis. The data highlight a BT/HSP70-SIRT7-CRY1 axis in regulating circadian phase coherence and glucose homeostasis.

Results

SIRT7 protein rhythm is clock-controlled

NAD⁺-dependent sirtuins are essential nutrient sensors that bridge circadian rhythms and metabolic processes in peripheral tissues, such as the mouse liver³⁵, while their nutrient-independent roles in the circadian clock are limited. We first examined sirtuin oscillations across a LD cycle in the murine liver. We observed prominent BMAL1 and CRY1 rhythmicity, as well as SIRT1, 3, 5, 6 and 7 (Fig. 1a,b). Of interest, SIRT7 and CRY1 protein levels were tightly correlated across the LD cycle: SIRT7 accumulated in the daytime but dropped at night (around *Zeitgeber* time [ZT] 12), while CRY1 exhibited the inverse pattern. Notably, *Sirt7* mRNA levels in the mouse liver lacked an obvious oscillation (Extended data Fig. 1a), and *Sirt7* mRNA and SIRT7 protein levels were almost undetectable in the hypothalamus (Extended data Fig. 1b,c).

Light represents the most prominent *Zeitgeber* of circadian clock. To further decipher the LD effect on SIRT7 protein expression, we examined the level of hepatic SIRT7 at ZT4 (day) and ZT16 (night) with or without a 2-h light pulse from ZT14 to ZT16 (L) in the dark period in mice fed *ad libitum*. We observed a dramatic reduction in Sirt7 expression at ZT16 compared to ZT4. Light exposure in the dark period elevated the level of SIRT7 but decreased that of CRY1 (Fig. 1c,d), suggesting that the LD cycle modulates SIRT7 levels. To examine whether SIRT7 rhythmicity is clock-controlled or induced by physiological changes upon light exposure, we switched the mice from LD to dark/dark (DD) condition. Consistent with the self-sustained property of the circadian clock, SIRT7 and CRY1 levels oscillated in a circadian manner in DD (Fig. 1e,f). These data suggest that SIRT7 protein oscillation is clock-controlled.

The peripheral clock is sensitive to feeding signals controlled by the SCN³⁶. Given the lack of SIRT7 in the hypothalamus, we reasoned that light might regulate hepatic SIRT7 via systemic cues, such as a feeding-fasting (FF) cycle. To test this possibility, we examined SIRT7 levels at ZT4 and ZT16 under feeding or fasting conditions (no food available from ZT0 to ZT16; NF), with a normal LD cycle or a 2-h light exposure (L) from ZT14 to ZT16. As shown, while fasting had little effect on hepatic SIRT7 levels in the dark period (ZT16NF Vs ZT16), SIRT7 levels markedly increased upon a 2-h light exposure (ZT16NF+L Vs ZT16NF) (Fig. 1g,h). This suggests that light resets SIRT7 expression pattern, independent of a FF cycle. In line with rhythmic SIRT7 expression, the level of H3K18ac, a direct target of SIRT7 deacetylase activity²⁷, exhibited a totally inversed oscillating pattern. By contrast, the protein levels of SIRT1, SIRT6 and their deacetylating target H3K9ac minimally changed between ZT4 and ZT16, regardless of feeding, fasting or light exposure. Though SIRT3, SIRT5 and BMAL1 oscillations were obvious between ZT4 and ZT16 in mice fed *ad libitum*, little change was observed during light exposure with or without fasting. Of note, the mRNA levels of *Sirt7*, *Cry1*, *Bmal1* and *Per2* in livers were hardly affected by light exposure in the dark period (Extended data Fig. 1d). Collectively, these data indicate that the rhythmicity of hepatic SIRT7 is entrained independent of FF.

Light-entrained BT oscillations regulate SIRT7 rhythmicity in the mouse liver

BT is a pivotal systemic entrainment cue used by the SCN to synchronize peripheral clocks^{14,19}. Murine BT can be elevated when environmental temperatures exceed the

thermoneutral zone (30°C)³⁷. Altering ambient temperature (AT) imparts changes in circadian gene expression in peripheral organs¹⁸. As BT oscillations were maintained during DD (Extended data Fig. 2a), we asked whether SIRT7 oscillation is regulated by BT. We subjected mice to a high AT (32°C) at different phases of the circadian cycle and measured body temperature. As expected, BT was high at ZT16 and low at ZT4 when mice were maintained at room temperature (Fig. 1i). High AT increased BT at ZT4 but not at ZT16, which correlates with down-regulated SIRT7 expression but increased CRY1 expression at ZT4 (Fig. 1j,k). By contrast, the cold exposure (4°C) at ZT16 decreased BT (Fig. 1l), increased SIRT7 but downregulated CRY1 expression (Fig. 1m,n).

Next, we examined whether light exposure at night stabilizes SIRT7 expression via BT. BT declined upon light exposure, but this was blocked by a concomitant high AT (Fig. 1o). Importantly, the light-induced increase in SIRT7 level at ZT16 was abolished by concomitant high AT challenge (Fig. 1p,q). Given that BT rhythmicity is regulated by feeding and locomotor activity³⁸, we examined the effects of fasting on BT oscillation. Indeed, the BT only exhibited a slight decline during fasting, but a dramatic decrease upon light exposure at ZT16 in fasted mice (Extended data Fig. 2b). Furthermore, we examined SIRT7 protein levels in fasted and re-fed mice after 24 h-fasting starting from ZT12. No significant change of SIRT7 protein levels was observed in mice liver tissues by fasting or refeeding (Extended data Fig. 2d). As a positive control, the p-AKT S473 level was reduced by fasting, and refeeding increased the p-AKT S473 level to a similar extent to the feeding group. Of note, the BT was dramatically reduced during light phase by 24 h-fasting (Extended data Fig. 2e). These findings support the notion that a light-driven BT oscillation regulates the rhythmicity of SIRT7 expression that is independent of an FF cycle.

HSP70 mediates SIRT7 degradation in the mouse liver

BT resets peripheral clocks via transcription factor HSF1, which drives the oscillation of heat-shock proteins (HSPs), including HSP70, HSPCA, HSP105 and HSPA8^{17,32}. We found that the mRNA levels of *Hsps* were significantly enhanced in the liver by high AT challenge at ZT4 (Extended data Fig. 2g). HSP70 is a key chaperone molecule that regulates protein homeostasis³⁹. Its protein level (low at ZT4 but high at ZT16) was negatively correlated with SIRT7 level (high at ZT4 but low at ZT16). We asked

whether BT regulates SIRT7 rhythmicity via HSP70. To answer this question, we did co-immunoprecipitation (Co-IP) experiments to determine any potential interaction between SIRT7 and HSP70 and found that SIRT7 interacts with HSP70 (Fig. 2a,b). Further degradation assay revealed that over-expression of HSP70 accelerated the degradation of HA-SIRT7 (Fig. 2c,d), which was blocked by the proteasome inhibitor MG132 (Fig. 2e,f). In addition, ectopic HSP70 enhanced HA-SIRT7 poly-ubiquitination (Fig. 2g). *Hsp70* knockdown (KD) by siRNA suppressed HA-SIRT7 degradation (Fig. 2h,i) and down-regulated HA-SIRT7 poly-ubiquitination (Fig. 2j). These indicate that HSP70 promotes SIRT7 degradation via the ubiquitin–proteasome system.

To ascertain the function of HSP70, we immunoprecipitated endogenous SIRT7 from liver lysates across a circadian cycle. A rhythmic interaction between HSP70 and SIRT7 was observed, with maximum binding at ZT12 and ZT16, consistent with high HSP70 levels but low SIRT7 in the dark period (Fig. 2k). We next tested whether HSP70-SIRT7 interaction is modulated by BT via examining the interaction at different AT. As shown, while a high AT increased HSP70 binding to SIRT7 at ZT4, a low AT reduced this interaction at ZT16 (Fig. 2l).

We then examined whether HSP70 is required for BT-generated SIRT7 rhythmicity. As shown, a 2-h heat shock (39.5°C) led to reduced SIRT7 expression but elevated HSP70 and CRY1 expression in mouse embryonic fibroblasts (MEFs) (Fig. 2m,n). *Hsp70* KD by siRNA in MEFs elevated SIRT7 but downregulated CRY1 protein levels. The effects of heat shock on SIRT7 and CRY1 levels were totally blocked in the case of *Hsp70* KD, suggesting that a high BT relies on HSP70 to down-regulate SIRT7 protein levels.

Next, we investigated whether BT regulates CRY1 via SIRT7, using a *Sirt7*^{-/-} mouse line generated by CRISPR/Cas9 procedure. We first noted that loss of *Sirt7* significantly up-regulated CRY1 protein level in MEFs (Fig. 2o,p). Interestingly, a 2-h heat shock up-regulated HSP70 expression in both wild-type (WT) and *Sirt7*^{-/-} MEFs, but the increase in CRY1 expression was only observed in WT. We next applied temperature challenges to *Sirt7*^{-/-} and WT mice. Again, an increase in CRY1 expression in *Sirt7*^{-/-} livers was observed (Extended data Fig. 3a,c). Consistent with the *in vitro* data, *Sirt7* depletion completely abolished high AT challenge-induced CRY1 up-

regulation at ZT4 in mouse livers (Extended data Fig. 3a). Similarly, the cold treatment-induced CRY1 down-regulation was not observed in *Sirt7*^{-/-} livers (Extended data Fig. 3c). HSP70 expression level was comparable in WT and *Sirt7*^{-/-} livers (Extended data Fig. 3a,c). Together, these data suggest that BT regulates SIRT7 protein stability through HSP70.

SIRT7 directly binds and deacetylates CRY1

We repeatedly observed that the CRY1 protein level is inversely correlated with SIRT7, peaking in the night but dropping in the daytime, and that *Sirt7* deficiency led to a dramatic increase in CRY1 protein in daytime. We speculated that SIRT7 might directly regulate CRY1. We first examined whether SIRT7 interact with CRY1. Co-IP revealed that SIRT7 interacted with CRY1 (Fig. 3a,b). Endogenous CRY1 was found in anti-SIRT7 immunoprecipitates (Fig. 3c). Finally, a GST pull down assay supported a direct interaction between His-CRY1 and GST-SIRT7 (Fig. 3d).

As a protein deacetylase⁴⁰, SIRT7 might deacetylate CRY1. As shown, HA-CRY1 acetylation levels were remarkably reduced in the presence of SIRT7 but were unaffected when co-transfected with catalytically inactive SIRT7 (H187Y) (Fig. 3e,f). Further, FLAG-CRY1 deacetylation was abolished in cells treated with nicotinamide (NAM), a pan sirtuin inhibitor (Fig. 3g,h). Thus, we conclude that SIRT7 deacetylase activity is required for CRY1 deacetylation. We also found that the CRY1 acetylation level was increased in *SIRT7* KO HEK293 cells (Fig. 3i,j). To test whether SIRT7 directly targets CRY1, we did an *in vitro* deacetylation assay. As shown, the acetylation level of FLAG-CRY1 was decreased in the presence of GST-SIRT7 and NAD⁺, and the decrease was blocked by NAM (Fig. 3k,l). Although CRY2 is a close homologue of CRY1, its acetylation level was hardly affected by NAM (Extended data Fig. 4a). We further examined whether other sirtuins affected acetylation of CRY1. As shown, only SIRT7 inhibited CRY1 acetylation (Extended data Fig. 4b). The data suggest that SIRT7 specifically deacetylates CRY1.

SIRT7 deacetylates CRY1 at K565/579

To identify the specific residues on CRY1 targeted for SIRT7-mediated deacetylation, we performed mass spectrometry. Three lysine (K) residues were found differentially acetylated, i.e. K22/565/579 (Supplementary Fig. 1). We generated non-acetylatable CRY1 mutants by replacing each lysine K22, K565 or K579 in turn with arginine (R).

Each mutant (FLAG-CRY1-KR) exhibited a comparable baseline acetylation level with WT (Fig. 3m,n). The effect of NAM on the various FLAG-CRY1-KR mutants was then examined. As shown, the NAM treatment enhanced the acetylation levels of WT and K22R but had a minimal effect on K565R and only a moderate effect on K579R (Fig. 3m,n), indicating that K565 and K579 are targeted by SIRT7 for deacetylation. We then generated FLAG-CRY1-2KR, wherein both K565 and K579 were mutated to R565 and R579, respectively. FLAG-CRY1-2KR displayed reduced acetylation levels compared to WT, and ectopic SIRT7 was unable to further downregulate the acetylation level (Fig. 3o,p). In addition, the acetylation level of FLAG-CRY1-2KR did not increase in *SIRT7* KO cells (Fig. 3q,r) or cells treated with NAM (Extended data Fig. 5), indicating that SIRT7 deacetylates CRY1 predominantly at K565 and K579.

SIRT7-mediated deacetylation destabilizes CRY1

In unsynchronized *SIRT7* KO HEK293 cells, the mRNA level of *CRY1* was slightly decreased, whereas the protein level was significantly increased (Extended data Fig. 6a-e). By contrast, CRY1 protein level was decreased in *SIRT7*-overexpressing cells (Extended data Fig. 6d,f). These findings indicate that SIRT7 most likely regulates CRY1 protein stability. Indeed, the FLAG-CRY1 degradation rate was accelerated in the presence of HA-SIRT7 compared to control (Fig. 4a,b), whereas the degradation of mutant CRY1 (FLAG-CRY1-2KR) was inhibited (Fig. 4c,d). Similar findings were observed for the endogenous CRY1 (Extended data Fig. 7a-d). Moreover, the CRY1 degradation rate was not affected in the presence of catalytically inactive mutant SIRT7 (H187Y) (Extended data Fig. 7e). As such, we propose that SIRT7 regulates CRY1 protein stability.

As CRY1 degradation was blocked by MG132, we reasoned that SIRT7 regulates CRY1 degradation via the ubiquitination–proteasome pathway. Indeed, ectopic expression of SIRT7 promoted poly-ubiquitination of CRY1 (Fig. 4e). Lysine acetylation enhances protein stability by blocking ubiquitination on the same residue⁴¹. K565/579 were previously identified as target ubiquitination residues of F-box and leucine rich repeat protein 3 (FBXL3), a subunit of ubiquitin protein ligase complex (SKP1-cullin-F-box, SCF)⁴²⁻⁴⁴. We speculated that SIRT7 might deacetylate CRY1 K565/579 to facilitate CRY1's ubiquitination by FBXL3 and subsequent degradation. Indeed, the ubiquitination level of FLAG-CRY1-2KR was dramatically reduced compared to WT

but remained unchanged upon SIRT7 over-expression (Fig. 4e).

To determine whether acetylation stabilizes CRY1, we investigated the ubiquitination and degradation rate of CRY1 in *SIRT7* KO HEK293 cells. As shown, the degradation of FLAG-CRY1 was significantly suppressed in *SIRT7* KO cells compared to control (Fig. 4f,g). By contrast, the degradation rate of FLAG-CRY1-2KR was comparable between *SIRT7* KO and control cells. Moreover, the poly-ubiquitination level of CRY1 was reduced in *SIRT7* KO cells (Fig. 4h). We asked whether the increased acetylation protects CRY1 from FBXL3-mediated degradation in *SIRT7* KO cells. As expected, FLAG-FBXL3 accelerated HA-CRY1 degradation, which was significantly attenuated in *SIRT7* KO cells (Fig. 4i,j). We further examined FBXL3-mediated CRY1 poly-ubiquitination in *SIRT7* KO cells. Although the poly-ubiquitination level of CRY1 was slightly increased upon FBXL3 overexpression in *SIRT7* KO cells, which is likely attributable to other lysine residues, the overall ubiquitination level of CRY1 was significantly lower in *SIRT7* KO cells compared with controls (Fig. 4k). These results demonstrate that increased CRY1 protein stability in *SIRT7* KO cells is due to elevated K565/579 acetylation, which prevents FBXL3-mediated ubiquitination and subsequent proteasomal degradation.

Finally, as AMPK also regulates the hepatic clock via phosphorylation-induced CRY1 degradation⁴⁵, we examined whether K565/579 deacetylation affects AMPK-mediated CRY1 degradation. As shown, the glucose starvation activated AMPK, which led to reduced protein levels of FLAG-CRY1 and FLAG-CRY1-2KR to a similar extent (Supplementary Fig. 2), indicating independent function of SIRT7 and AMPK in the regulation of CRY1 stability.

SIRT7 regulates the circadian phase of hepatic clocks

The data thus far suggest an essential role for SIRT7 in hepatic clocks, as confirmed by that deletion of *Sirt7* led to a dramatic increase in CRY1 expression at ZT0 and ZT6 in mouse livers (Fig. 5a,b). We confirmed that hepatic CRY1 was acetylated in a cyclic manner, peaking at ZT12-ZT18 in WT mice; this oscillation was, however, disrupted in *Sirt7*^{-/-} mice with elevated acetylation at ZT0-ZT6 (Fig. 5c,d). We asked whether SIRT7 regulates core clocks in a cell autonomous manner. Indeed, a reduced amplitude of *Bmal1*, *Cry1*, *Dbp*, *Rev-Erba* and *Reverbβ* mRNA levels was observed in *Sirt7*^{-/-} MEFs compared to WT (Extended data Fig. 8a). Moreover, the protein level of CRY1

was significantly elevated, whereas that of BMAL1 was reduced in *Sirt7*^{-/-} cells (Extended data Fig. 8b,c). The circadian phase of *Per2* was significantly delayed in *Sirt7*^{-/-} MEFs. These data implicate that SIRT7 regulates the expression of endogenous core clock proteins.

Next, we examined the mRNA levels of core clock genes in *Sirt7*^{-/-} livers. As shown, *Sirt7* deficiency slightly downregulated the mRNA levels of *Bmal1*, *Rev-Erbβ* and *Dbp* but not *Per2* or *Rev-Erba* (Fig. 5e). Though the amplitude of the *Cry1* daily oscillation was virtually unchanged, its mRNA level was reduced in *Sirt7*^{-/-} livers specifically in the light phase. Of particular interest, the circadian phases of *Bmal1*, *Cry1*, *Rev-Erbβ* and *Dbp* were substantially advanced, whereas that of *Per2* was delayed in *Sirt7*^{-/-} livers compared to WT. No circadian phase shift in *Bmal1*, *Cry1*, *Dbp* or *Per2* was observed in the hypothalamus of *Sirt7*^{-/-} mice (Extended data Fig. 9). These data suggest that SIRT7 regulates the circadian phase of hepatic clocks.

Acute ambient temperature changes circadian phase of hepatic clock

Our data so far suggest a BT/HSP70-SIRT7-CRY1 axis in the regulation of hepatic clock. Acute AT challenge affected SIRT7 and CRY1 levels in mouse livers. We next examined whether various AT conditions modulates hepatic clock. High temperature treatment increased the protein level of HSP70 but decreased that of SIRT7; by contrast, the cold temperature treatment elicited opposite effect (Fig. 6a-c). Both high and low temperature dampened the oscillation of BT and HSP70 and SIRT7 protein levels. Interestingly, consistent with low level of SIRT7, high temperature treatment led to accumulation of CRY1 at ZT5 and ZT9, which is quite similar to that in *Sirt7*^{-/-} liver. By contrast, CRY1 level was reduced at ZT17 at cold temperature compared to RT, probably owing to constitutive high SIRT7 level in the liver. Likely attributable to feedback repression of itself, *Cry1* mRNA level was increased at cold temperature but reduced at high temperature (Fig. 6d). While cold temperature increased *Bmal1* gene expression, both protein and mRNA levels of BMAL1 were reduced at high temperature. The protein level of PER2 was reduced at ZT21 at high temperature, but *Per2* mRNA level was significantly reduced at ZT13 and ZT17. By contrast, cold temperature treatment led to increased expression of *Per2* at ZT5 and ZT9 but hardly affected the protein. Again, similar to *Sirt7* deficiency, both cold and high temperature attenuated the oscillation of *Dbp* and *Rev-erbβ*. The circadian phases of *Bmal1*, *Cry1*, *Per2*, *Rev-*

Erbβ and *Dbp* were all advanced upon both high and cold treatment. These results indicate that acute temperature challenge modulates circadian phase of liver clock.

We further examined the effect of long-term acclimation to AT challenges. The mice were acclimated at different ATs for one week. High temperature treatment only slightly increased the BT at light phase and attenuated its oscillation (Extended data Fig. 10a). Cold temperature treatment decreased the BT and also slightly attenuated the oscillation. The protein levels and circadian phases of HSP70 and SIRT7 were accordingly changed between high/cold and room temperature (Extended data Fig. 10b,c), but less obvious compared to that in the acute treatment (see Fig. 6b,c). Of note, low AT increased protein level of SIRT7 but decreased that of HSP70 at ZT13 and ZT17 compared to room temperature. The expression levels and circadian phases of *Bmal1*, *Per2* and *Rev-erbβ* mRNAs were merely changed at different conditions (Extended data Fig. 10d). High temperature delayed circadian phase of *Rev-erba*, and increased expression level of *Dbp*. While circadian phases of *Cry1* mRNA were advanced at high and cold temperature compared with that at room temperature, circadian phase of CRY1 protein were delayed (Extended data Fig. 10b-d). We noticed that little difference in circadian locomotor activity was observed at different conditions (Extended data Fig. 10e,f).

SIRT7 counteracts with hepatic clock phase entrainment by restricted feeding

The circadian phase of hepatic clocks is coordinated by systemic cues from the central pacemaker and feeding activity. The SCN-orientated synchronizing signal counteracts feeding-induced phase entrainment of hepatic clocks³⁴. Given the critical role for SIRT7 in the SCN-driven synchronization of hepatic clocks and advanced circadian phase of core clock genes in *Sirt7*^{-/-} livers, we reasoned that SIRT7-mediated synchronizing cues from the central pacemaker might counteract the feeding cues in the circadian phase entrainment of hepatic clocks. To test this hypothesis, *Sirt7*^{-/-} and WT control mice were subjected to daytime-restricted feeding (RF) (Fig. 7a). After 2 days of RF (RF2), the circadian phases of *Bmal1*, *Cry1*, *Rev-erba*, *Rev-erbβ* and *Dbp* were slightly changed in WT mice. Intriguingly, the circadian phases adapted to RF more rapidly in *Sirt7*^{-/-} mice. For instance, *Bmal1*, *Cry1* and *Rev-erba* levels showed a circadian phase advance of up to 8 h in *Sirt7*^{-/-} mice, whereas such a phase shift was <4 h in mice fed *ad libitum*. Although two peaks of *Per2* expression were observed at

ZT4 and ZT16 in WT mice, a new phase of *Per2* already appeared after RF2 in *Sirt7*^{-/-} mice whereby its expression peaked at ZT4. 4 days after RF (RF4), the circadian phase of all examined clock genes had completely reversed, and difference was hardly observed between *Sirt7*^{-/-} and WT mice. This finding suggests that SIRT7 counteracts the phase entrainment of hepatic clocks by RF.

The reversal of phase of core clock genes in WT mice after RF4 (Fig. 7a) prompted us to investigate whether the BT/HSP70-SIRT7 axis is involved in resetting the phase of core clocks during RF. We found that BT oscillations were still maintained after RF2, but the level was significantly increased at ZT20 compared with feeding *ad libitum* (Fig. 7b). However, BT oscillations were completely abolished after 4 days, with a constitutive high BT. We measured HSP70, SIRT7 and CRY1 protein levels. Consistent with changes in BT, after RF2, HSP70 and SIRT7 levels were altered at ZT20, and the circadian phase of CRY1 was slightly delayed (Fig. 7c,d). After RF4, HSP70 and SIRT7 protein levels lost rhythmicity and became constitutively high or low, respectively, across a circadian cycle. Meanwhile, CRY1 level was high after RF4 compared with feeding *ad libitum*, but the oscillation was attenuated. We further examined BT and HSP70 levels in *Sirt7*^{-/-} mice during RF. As shown, *Sirt7* deficiency had little effect on BT and HSP70 levels (Fig. 7f-i and Supplementary Fig. 3), suggesting a downstream role of SIRT7 in the BT/HSP70-SIRT7 axis. The difference in CRY1 level between *Sirt7*^{-/-} and WT mice was prominent in the light period after 2 days, but this effect became negligible after RF4. These data imply that the BT/HSP70-SIRT7 axis counteracts the circadian phase resetting induced by RF.

SIRT7 regulates rhythmic hepatic gluconeogenesis

Though the phase of hepatic clock genes was reversed after RF4 compared to Ad, the rhythmicity of the BT/HSP70-SIRT7 axis was completely abolished at RF4. RF can downregulate blood glucose⁴⁶ and CRY1 regulates circadian gluconeogenesis^{47,48}. The constant high level of CRY1 expression induced by RF and *Sirt7* deficiency prompted us to investigate whether SIRT7 and CRY1 cooperate to regulate glucose homeostasis. To this end, we first examined blood glucose levels in mice fed *ad libitum*. The blood glucose level oscillated, with a trough at ZT1 and peak at ZT13 in WT mice (Fig. 8a). By contrast, attenuated blood glucose oscillations were observed in *Sirt7*^{-/-} mice, and glucose levels were significantly reduced at ZT5 and ZT9. Of note, the overall blood

glucose level was attenuated in *Sirt7*^{-/-} mice. The blood glucose oscillation was also attenuated in WT mice at RF2, with a moderate glucose level maintained across the whole day. By contrast, the oscillation pattern of blood glucose levels was almost reversed in *Sirt7*^{-/-} mice. Notably, the blood glucose level was low from ZT5 to ZT13 in *Sirt7*^{-/-} mice compared to WT. The oscillation pattern in glucose levels was totally reversed in both genotypes at RF4, peaking at ZT1. At this stage, little difference was observed in the oscillation pattern and in the overall blood glucose levels between WT and *Sirt7*^{-/-} mice, implicating an important role for SIRT7 in regulating RF-induced blood glucose reduction.

Previous study indicates that loss of *Sirt7* improved insulin resistance and suppressed blood glucose levels during high-fat diet (HFD) conditions⁴⁹. We thus performed glucose tolerance test (GTT) and pyruvate tolerance test (PTT) in WT and *Sirt7*^{-/-} mice with normal feeding conditions (Fig. 8b). The GTT data indicated better glucose tolerance in *Sirt7*^{-/-} mice compared to WT and the PTT suggested inhibition of gluconeogenesis in *Sirt7*^{-/-} mice. Rhythmic hepatic gluconeogenesis is controlled by cryptochromes^{47,48}, partially by inhibiting glucagon-CREB pathway. We examined phospho-CREB during RF. The level of p-CREB peaked at ZT4 and ZT8 in the Ad scenario (Fig. 8c,d). At RF2 and RF4, the peaking levels of p-CREB were observed at ZT0 and ZT20, suggesting that the glucagon-CREB pathway were rapidly reversed during RF. Meanwhile, the level of p-CREB was comparable between WT and *Sirt7*^{-/-} mice. In addition, serum insulin and glucagon levels and food intake were not much changed in *Sirt7*^{-/-} mice compared to WT (Fig. 8e-g), suggesting that reduced blood glucose levels in *Sirt7*^{-/-} mice is most likely attributable to suppressed hepatic gluconeogenesis.

To further determine whether the reduced blood glucose level in *Sirt7*^{-/-} mice was due to hepatic gluconeogenesis, we generated a *Sirt7*^{fl/fl} conditional KO line and injected an adenoviral vector expressing Cre recombinase driven by cytomegalovirus promoter via tail vein. *Sirt7* was largely depleted (> 90% reduction) in the livers of *Sirt7*^{fl/fl} mice (LS7KO hereafter) but not in *Sirt7*^{+/+} mice (Fig. 8h,i). By contrast, SIRT7 was hardly deleted in other tissues/organs (Fig. 8j), probably owing to high tropism of adenovirus for hepatocytes^{50,51}. Consistent with whole body *Sirt7*^{-/-} mice, low blood glucose level was observed in LS7KO mice when fed *ad libitum* or RF2 (Fig. 8k). GTT and PTT

assays implicate that hepatic gluconeogenesis is responsible for reduced glucose level in *Sirt7*^{-/-} mice (Fig. 8). The data suggest that SIRT7 regulates hepatic gluconeogenesis during the light/resting period.

Altogether, we showed that BT cycles generated by the central clock induce rhythmic transcription of HSP70 in the mouse livers, which promotes SIRT7 ubiquitination and proteasomal degradation. SIRT7 then deacetylates and promotes FBXL3-mediated CRY1 ubiquitination and degradation, integrating the central pacemaker to hepatic clock. In mouse liver, SIRT7 is required to maintain glucose homeostasis during the light/resting period (Fig. 9).

Discussion

The SCN is the master circadian pacemaker and is entrained by LD cycles. Peripheral cells possess circadian clocks, which are crucial for local physiology, such as glucose homeostasis in the liver. The SCN synchronizes peripheral clocks through different pathways including hormonal, nervous signal, BT cycles and feeding activities^{17-19,32}. Interestingly, these signals conveyed by the SCN seem to counteract with FF cycle, which serves as an independent dominant *Zeitgeber* of peripheral clocks^{34,52}. RF in daytime leads to reversed core clock gene expression in peripheral tissues^{22,53-55}. Though the molecular mechanisms by which feeding regulates local clock have been demonstrated², how feeding defeats the SCN-derived signals during RF is still largely unknown. Here, we revealed SIRT7 as an early element responsive to light, transmitting timing information to the mouse liver. Like the SCN-lesioned animals, the kinetics of RF-mediated phase-shifting is accelerated in *Sirt7*^{-/-} livers. In mice fed *ad libitum*, *Sirt7* depletion shifts the circadian phase of the liver but not of the hypothalamus, in the latter of which *Sirt7* is hardly detected. Previous studies have shown that *Bmal1* and *Per2* are differentially controlled by the SCN and food-derived resetting cues^{34,53}, respectively. We found that SIRT7 in the liver is stabilized by light but is independent of BMAL1 and PER2, implicating SIRT7 as an early element responsive to light in the liver. SIRT7 was increased at ZT16 upon light exposure in fasted mice, supporting an essential role for the LD cycle rather than food availability in driving rhythmic SIRT7 expression.

BT is a common resetting cue utilized by the SCN to entrain peripheral clocks^{17-19,32}.

HSF1 is essential in resetting peripheral clocks via BT, and *Hsps* transcription is driven by HSF1 in a circadian manner^{17,32}. At the molecular level, however, the connection between BT and local clock components is still largely unknown. Our results indicate that HSP70, a key molecular chaperone, interacts and promotes SIRT7 ubiquitination and proteasomal degradation. SIRT7 deacetylates CRY1 at K565/579 residues, two of 10 cryptochrome lysines targeted for FBXL3-mediated ubiquitination and degradation⁴²⁻⁴⁴. Constitutive high level of CRY1 might suppress its own transcription in *Sirt7*^{-/-} mice, specifically in the light phase of a circadian cycle. Similar to *Sirt7* deficient mice, a delayed circadian phase of *Per2* was observed in *Fbxl3*^{-/-} livers^{56,57}, supporting the notion that the disrupted circadian phase phenotype of *Sirt7*^{-/-} mice is attributable, at least partially, to dysregulated CRY1. Thus, the BT/HSP70-SIRT7-CRY1 axis integrates systemic BT to hepatic clock. Consistently, acute temperature challenge significantly interferes the oscillation and circadian phase of core clocks in liver. Cold temperature treatment enhanced oscillation of *Bmal1*, *Cry1*, and *Per2*. By contrast, the amplitude of *Rev-erba/β* and *Dbp* was reduced, suggesting that clock genes are differentially regulated by BT. Moreover, the cold temperature treatment led to increased mRNA levels of *Per2* at ZT4 and ZT8 but change at protein levels was merely observed. We speculate that in addition to transcriptional regulation, hepatic PER2 is predominantly controlled at post-transcriptional and post-translational levels. High temperature led to dampened oscillation of SIRT7 with constitutively reduced protein levels across the circadian cycle. Similar to *Sirt7*-KO mice, the advanced circadian phases of *Bmal1*, *Cry1*, *Dbp* and *Rev-erbb* were observed at high AT compared with room AT. Very interestingly, long-term acclimation of AT challenge elicits quite different effect on hepatic clock compared to that of acute challenge, which might be owing to rescued oscillation of BT and HSP70 and SIRT7 protein levels. It is plausible to speculate that the central circadian system might engage metabolic reprogramming and/or temperature compensation to adapt AT changes.

Mammalian cryptochrome shares a conserved photolyase-homology at the N-terminus, but a divergent carboxyl tail domain (CTD)⁵⁸⁻⁶⁰. Though it is generally accepted that CTD is crucial for cryptochrome functional diversity^{59,61}, the molecular mechanisms are not well understood. Our results demonstrate that CRY1 but not CRY2, is deacetylated by SIRT7, as the K565/579 residues are only present in CRY1. The data shed new light on functional importance of the CTD for CRY1 stability mediated by

SIRT7 deacetylase. In addition, CRY1 protein stability is also regulated by AMPK-mediated phosphorylation⁴⁵. Our data implicate that SIRT7 and AMPK regulate CRY1 protein stability via independent pathways, involving ubiquitination at different residues.

The SCN also indirectly regulates daily rhythms of BT via feeding/activity³⁸. Under normal feeding conditions, elevated BT in the dark phase is attributable to increased activity and diet-induced thermogenesis⁶². We demonstrated that BT is not strongly changed in the dark phase in fasted mice (Extended data Fig. 2). Interestingly, a previous study found that BT was not affected in the dark phase after food deprivation, likely due to maintained activity in the dark phase⁶³. During prolonged feeding in the daytime, food-entrainable oscillator (FEO) overcomes the effects of the SCN, and acts as the master pacemaker^{38,62}. FEO-controlled food-anticipatory activity (FAA) leads to increase of BT preceding the feeding time⁶². Meanwhile, feeding signals regulate diet-induced thermogenesis in the ventromedial hypothalamus (VMH) and contribute to the constitutive high BT during daytime⁶⁴⁻⁶⁷. It explains why the SCN-controlled BT oscillation was blocked at RF4, suggesting that BT-mediated synchronization of peripheral tissues is lost.

Disrupted circadian rhythms leads to metabolic disturbances^{30,68}. Long-term RF leads to metabolic disturbance with reduction of blood insulin and increase of glucagon and free fatty acid^{55,69}, which can be rescued by glucose administration^{55,69}. The circadian control of gluconeogenesis is complicated: multiple pathways are involved, including local clock components (cryptochrome), feeding signals (insulin and glucagon), the SCN-controlled corticosterone and autophagy^{47,48,70}. Our data indicate that RF leads to constitutively high BT and HSP70, which disrupt SIRT7 oscillation, and subsequently lead to an increase in CRY1 level. CRY1 regulates hepatic gluconeogenesis by different pathways, i.e. glucagon-CREB and glucocorticoid pathways. Cytoplasmic CRY1 inhibits glucagon-CREB pathway during feeding time (ZT13)⁴⁸, whereas nuclear CRY1 interacts with glucocorticoid receptor (GR) and inhibits gluconeogenesis⁴⁷. Our results suggest that glucagon-CREB pathway less likely contributes to attenuated gluconeogenesis by *Sirt7* deficiency. As SIRT7 is predominantly localized in the nucleus^{71,72}, we reason that other pathways might be involved.

The role of SIRT7 in hepatic glucose metabolism is seemingly controversial^{49,73}. Loss

of *Sirt7* protects from high-fat-diet-induced hyperglycemia in mice. Consistently, our data revealed suppressed gluconeogenesis and improved glucose tolerance in *Sirt7*^{-/-} and LS7KO mice. Interestingly, better glucose and insulin tolerance has been reported in *Sirt7*^{-/-} mice fed a high-fat diet (HFD), which is most likely attributable to increased glucose disposal rate⁴⁹. The mechanisms of HFD-induced hyperglycemia and insulin resistance are complicated. SIRT7 also mediates adipogenesis and lipid metabolism, which may contribute to the pathological process^{49,74}. Nevertheless, our results indicate that SIRT7 is required for the rhythmic hepatic gluconeogenesis. More importantly, SIRT7 couples BT and hepatic gluconeogenesis. Disruption of BT are occurred in diabetes mellitus and aging^{75,76}. Altering BT might be critical to maintain the robustness of peripheral clocks, providing chronotherapeutic strategy to prevent metabolic diseases and aging.

Collectively, we reveal a novel molecular network, i.e. BT/HSP70-SIRT7-CRY1 axis, wherein SIRT7 couples systemic BT cues to hepatic oscillators via HSP70 and ensures circadian phase coherence and glucose homeostasis in the liver.

Methods

Animals

Sirt7-knockout (KO) alleles were created by CRISPR/Cas9-mediated genome editing in C57BL/6 mice via transgenic animal services from Cyagen. Briefly, the Cas9 mRNA and *Sirt7*-gRNA were generated by *in vitro* transcription and co-injected into fertilized eggs. Successful deletion was confirmed by polymerase chain reaction (PCR) and DNA sequencing. *Sirt7* heterozygous males were backcrossed with C57BL/6 females for at least five generations to preclude off-targeted mutations. The sequence of the gRNA was as follows, 5'-CTTGGCCGAGAGCGAGGATC-3'. Establishment of the *Sirt7^{flox/flox}* mice was performed according to the method described in a previous report⁴⁹ via transgenic animal services from Shanghai Model Organisms Center, Inc. Briefly, *LoxP* sites were inserted into introns 5 and 9, respectively. The CMV-Cre adenovirus was purchased from HanBio Technology. Male, 8-10-week-old *Sirt7^{+/+}* and *Sirt7^{flox/flox}* littermates were injected via the tail vein with 100 μ l of adenoviral-Cre ($1-2 \times 10^{10}$ pfu/ml). The mice were maintained on a 12-h light/dark cycle (150 lux at the cage level from white LED lamps) at 22°C with access to a standard diet (70% kcal carbohydrates, 20% kcal protein, and 10% kcal fat, Beijing Keao Xieli Feed Co.,Ltd.) and water *ad libitum*. Male mice aged 8-12 weeks with littermate controls were used in all experiments. For temperature challenge, the mice were first placed in individual cages without nesting material and allowed to acclimated at 22°C for at least 4 weeks in temperature-controlled incubators. The body temperature was measured using an infrared camera FLIRE6 (FLIR Systems, USA). The mean temperature from all over the body was calculated. Rectal temperatures were measured using a Thermocouple Meter (Landwind medical Industry Co., Ltd). For time-restricted feeding, *Sirt7^{-/-}* and WT control mice were fed *ad libitum* for 3 weeks, and then subjected to restricted feeding (RF) in which food was only available during daytime. Mice were sacrificed every 4 h after the inversion of feeding regimen on either the second or fourth day. The kinetics of circadian phase shifting were determined by analyzing mRNA levels of clock genes by real-time PCR. All animals were housed and handled in accordance with protocols approved by the Committee on the Use of Live Animals in Teaching and Research.

Cell culture

HEK293 were cultured in DMEM (Life Technologies), supplemented with 10% fetal bovine serum (FBS), 100 U/ml penicillin and 100 mg/ml streptomycin, and maintained in a humidified incubator at 37°C with 5% CO₂. Primary MEFs were prepared from E13.5 embryos of *Sirt7*^{+/-} pregnant mice as described previously⁷⁸. Briefly, after removing the head and internal organ, the embryos were trypsinized for 20 min, and seeded in T-25 cell culture dishes. Primary MEFs were grown in DMEM supplemented with 15% FBS, 10 mM HEPES (pH 7.0), 2 mM glutamine (Life Technologies), 8 mM nonessential amino acids (Life Technologies), 1 mM sodium pyruvate (Life Technologies). The cells were transfected with the indicated constructs using Lipofectamine[®]3000 reagent (Invitrogen), according to the manufacturer's protocols. Cycloheximide (CHX, 50 µg/ml, Sigma-Aldrich), MG132 (20 µM, 6 h, Sigma-Aldrich), and nicotinamide (NAM, 10 mM, 6 h, Sigma-Aldrich) were added to the cultures as indicated.

Plasmids

The FLAG-SIRT7, FLAG-CRY1 HA-SIRT7 and HA-CRY1 constructs were established as follows: The full length coding sequences of human CRY1 and SIRT7 were amplified from the cDNA of HEK293 cells by real-time-PCR; the PCR products were cloned between the *Xho*I and *Xba*I or *Bam*HI and *Xho*I sites in the pcDNA3.1 vector. FLAG-SIRT7 H187Y was purchased from Addgene (#53151). FLAG-His-HSP70 (#CH833663), FLAG-His-CRY2 (#CH872052) and FLAG-His-FBXL3 (#CH804377) were purchased from ViGene Biosciences, Inc. Various KR mutations were introduced via PCR-based site-directed mutagenesis. The Myc-Ub construct was provided by Dr Z.J. Zhou (School of Biomedical Sciences, LKS Faculty of Medicine, University of Hong Kong, Hong Kong).

CRISPR/Cas9-mediated gene deletion

CRISPR/Cas9-mediated gene deletion was conducted as previously described⁷⁹. In brief, guide RNA targeting SIRT7 was subcloned into the PX459 vector (Addgene; #48139). The HEK293 cells were transfected with 1 µg PX459-gSirt7. After 48 h, clones were selected with 1 µg/ml puromycin (Invitrogen), and then expanded for further analysis. The mutations were confirmed by PCR, DNA sequencing and immunoblotting. To avoid non-specific off-target effects, two independent gRNAs were used, the sequences were as follows: gSirt7-1-forward (F): 5'-

CACCGCCGCGCTTTGCGCTCGGAG-3’,
gSirt7-1-reverse (R): 5’-AAACCTCCGAGCGCAAAGCGGCGGC-3’;
gSirt7-2-F: 5’-CACCGTGTGTAGACGACCAAGTATT-3’,
gSirt7-2-R: 5’-AAACAATACTTGGTCGTCTACACAC-3’.

Antibodies, immunoprecipitation and western blotting

Anti-FLAG and Anti-HA antibodies were purchased from Sigma-Aldrich. The antibodies used for immunoblotting included anti-SIRT1 (#8469, Cell Signaling Technology, Inc.), anti-SIRT2 (ab67299, Abcam), anti-SIRT3 (#5490, Cell Signaling Technology, Inc.), anti-SIRT4 (Sigma), anti-SIRT5 (ab108968, Abcam), anti-SIRT6 (NB100-2252, Novus), anti-SIRT7 (sc-135055, Santa Cruz Biotechnology, Inc.), anti-BMAL1 (ab93806, Abcam), anti-CRY1 (ab3518, Abcam), anti-PER2 (sc-25363, Santa Cruz Biotechnology, Inc.), anti-HSP70 (#4872, Cell Signaling Technology, Inc.), anti-ubiquitin (#3936, Cell Signaling Technology, Inc.), anti- α -tubulin (#AT819-1, Beyotime Biotechnology, Inc.), anti-GST (#2624, Cell Signaling Technology, Inc.), anti-His and pan acetyl lysine antibody (PTM-101, PTM-105, PTM-Biolab). p-CREB Ser133 (#9198, Cell Signaling Technology, Inc.) and p-AKT Ser473 (#3787, Cell Signaling Technology, Inc.). The primary antibodies used for immunoprecipitation included anti-FLAG M2 Affinity Gel (Sigma-Aldrich), monoclonal anti-HA Agarose (Sigma-Aldrich), anti-SIRT7 (sc-365344, Santa Cruz Biotechnology, Inc.) and anti-CRY1 (ab3518, Abcam). The secondary antibodies used for endogenous immunoprecipitation included Rabbit Anti-Mouse IgG (Light Chain Specific) and Mouse Anti-Rabbit IgG (Light-Chain Specific) (#58802, #93702, Cell Signaling Technology, Inc.).

Whole-cell extracts were prepared in immunoprecipitation (IP) lysis buffer (20 mM Tris-HCl, pH 8.0, 250 mM NaCl, 0.2% NP-40, 10% glycerol, 2 mM EDTA, 1 mM PMSF and protease inhibitor cocktail). For immunoprecipitation, whole-cell lysates were mixed with 2 μ g primary antibody as indicated, or control IgG and precipitated using Protein A/G agarose beads (Thermo Fisher). To evaluate the acetylation of CRY1, whole-cell extracts were prepared in IP lysis buffer supplemented with 10 mM sodium butyrate (NaB) and 10 mM NAM. Equal quantities of cell lysates or immunoprecipitated protein samples were separated by SDS-PAGE and transferred onto a PVDF membrane (Millipore). The primary antibodies were added and incubated

at 4°C overnight. Following incubation with secondary antibodies conjugated to HRP (Jackson Laboratories), the signal was visualized using an enhanced ECL chemiluminescence detection system (Sage Creation Science).

RNA extraction and RT-PCR analysis

Total RNA were extracted using TRIzol[®] reagent (Invitrogen). Complementary DNA was synthesized from 2 µg RNA using Primescript[®] RT Master kit (Takara, Japan) according to the manufacturer's protocol. Quantitative RT-PCR was performed on a BIO-RAD CFX Connect[™] Real-time PCR system with SYBR Ex Taq Premixes (Takara). The relative quantification Delta-delta Ct method was used for analysis. Mouse *36b4* and human *ACTIN* were used as internal controls to normalize all data. The primers are listed in Table S1.

GST-pull down assay

GST-pull down assay was performed using recombinant GST-SIRT7 and His-CRY1 purified from BL21 *E. coli*. GST or GST-CRY1 protein (2 µg) was immobilized on Glutathione-Sepharose 4B and incubated with His-CRY1 in GST binding buffer (20 mM Tris-HCl [pH 7.4], 0.1 mM EDTA, and 150 mM NaCl, 0.2% NP-40, protease inhibitors cocktail). The beads were washed three times with GST wash buffer (20 mM Tris-HCl [pH 7.4], 0.1 mM EDTA, and 250 mM NaCl, and 0.2% NP-40). Bead-bound CRY1 was analyzed by SDS-PAGE and western blotting. For purification of recombinant His-CRY1 from BL21 *E. coli*, 1 mM flavin adenine dinucleotide (FAD) was added to the lysis buffer (50 mM PBS [pH 7.4], 0.5 M NaCl, 1 mM PMSF, and protease inhibitors cocktail).

***In vitro* deacetylation assay**

FLAG-CRY1 was overexpressed in HEK293 cells and immunoprecipitated on the Anti-FLAG M2 Affinity Gel (Sigma-Aldrich). For the deacetylation assay, purified FLAG-CRY1 was incubated with 1 µg GST-SIRT7 in deacetylation buffer (50 mM Tris-HCl [pH 8.0], 4 mM MgCl₂, 0.2 mM DTT, 1 mM NAD⁺, and protease inhibitors cocktail) for 30 min with constant agitation. The acetylation level of CRY1 was monitored by western blotting using anti-acetyl lysine antibodies.

Mass spectrometry

The gel lanes were cut from the gel and subjected to in-gel digestion with trypsin. The digested peptides were resuspended and analyzed by LC-MS with a QTRAP 6500 mass spectrometer (Applied Biosystems). Data analysis was performed using the Mascot search engine against IPI-HUMAN and NCBI databases for protein identification.

Metabolic analysis

For glucose measurement, the mice were fasted overnight. For GTT, glucose (1 g/kg) was intraperitoneally (i.p.) injected. For PTT, pyruvate (2 g/kg) was i.p. injected. Glucose levels were measured using a glucometer (Onetouch Ultravue, Johnson, USA) at indicated time points. The serum insulin levels were measured using a Mouse UltraSensitive Insulin Jumbo ELISA kit (ALPCO, USA). Glucagon levels in serum were measured using a Glucagon Quantikine ELISA kit (R&D Systems, USA).

Statistical analysis

Data are presented as the means \pm standard error of the mean. Statistical analyses were performed using GraphPad Prism (version 6.0, GraphPad Software, Inc.). Statistical tests were two-tailed Student's *t*-test (for comparison between two groups) or two-way analysis of variance followed by Bonferroni's multiple comparisons test (for comparison among three groups or in two groups at multiple time points). * $P < 0.05$ was considered to indicate a statistically significant difference.

Reporting Summary: Further information on research design is available in the Nature Research Reporting Summary linked to this article.

Data Availability

The authors declare that all the data supporting the findings of this study are available from the corresponding authors on reasonable request.

References

1. Marcheva, B., *et al.* Disruption of the clock components CLOCK and BMAL1 leads to hypoinsulinaemia and diabetes. *Nature* **466**, 627-631 (2010).
2. Panda, S. Circadian physiology of metabolism. *Science* **354**, 1008-1015 (2016).
3. Reick, M., Garcia, J.A., Dudley, C. & McKnight, S.L. NPAS2: An analog of clock operative in the mammalian forebrain. *Science* **293**, 506-509 (2001).
4. DeBruyne, J.P., Weaver, D.R. & Reppert, S.M. CLOCK and NPAS2 have overlapping roles in the suprachiasmatic circadian clock. *Nat Neurosci* **10**, 543-545 (2007).
5. van der Horst, G.T.J., *et al.* Mammalian Cry1 and Cry2 are essential for maintenance of circadian rhythms. *Nature* **398**, 627-630 (1999).
6. Kume, K., *et al.* mCRY1 and mCRY2 are essential components of the negative limb of the circadian clock feedback loop. *Cell* **98**, 193-205 (1999).
7. Bunger, M.K., *et al.* Mop3 is an essential component of the master circadian pacemaker in mammals. *Cell* **103**, 1009-1017 (2000).
8. Gekakis, N., *et al.* Role of the CLOCK protein in the mammalian circadian mechanism. *Science* **280**, 1564-1569 (1998).
9. Takahashi, J.S., Hong, H.K., Ko, C.H. & McDearmon, E.L. The genetics of mammalian circadian order and disorder: implications for physiology and disease. *Nat Rev Genet* **9**, 764-775 (2008).
10. Preitner, N., *et al.* The orphan nuclear receptor REV-ERB alpha controls circadian transcription within the positive limb of the mammalian circadian oscillator. *Cell* **110**, 251-260 (2002).
11. Sato, T.K., *et al.* A functional genomics strategy reveals Rora as a component of the mammalian circadian clock. *Neuron* **43**, 527-537 (2004).
12. Solt, L.A., *et al.* Regulation of circadian behaviour and metabolism by synthetic REV-ERB agonists. *Nature* **485**, 62-68 (2012).
13. Dibner, C., Schibler, U. & Albrecht, U. The Mammalian Circadian Timing System: Organization and Coordination of Central and Peripheral Clocks. *Annual Review of Physiology* **72**, 517-549 (2010).
14. Mohawk, J.A., Green, C.B. & Takahashi, J.S. Central and Peripheral Circadian Clocks in Mammals. *Annu Rev Neurosci* **35**, 445-462 (2012).
15. Orozco-Solis, R., *et al.* The Circadian Clock in the Ventromedial Hypothalamus Controls Cyclic Energy Expenditure. *Cell Metab* **23**, 467-478 (2016).
16. Gerhart-Hines, Z., *et al.* The nuclear receptor Rev-erb alpha controls circadian thermogenic plasticity. *Nature* **503**, 410-+ (2013).
17. Saini, C., Morf, J., Stratmann, M., Gos, P. & Schibler, U. Simulated body temperature rhythms reveal the phase-shifting behavior and plasticity of mammalian circadian oscillators. *Genes Dev* **26**, 567-580 (2012).
18. Brown, S.A., Zumbrunn, G., Fleury-Olela, F., Preitner, N. & Schibler, U. Rhythms of mammalian body temperature can sustain peripheral circadian clocks. *Curr Biol* **12**, 1574-1583 (2002).
19. Buhr, E.D., Yoo, S.H. & Takahashi, J.S. Temperature as a Universal Resetting Cue for Mammalian Circadian Oscillators. *Science* **330**, 379-385 (2010).

20. Fonken, L.K., *et al.* Light at night increases body mass by shifting the time of food intake. *Proc Natl Acad Sci U S A* **107**, 18664-18669 (2010).
21. Stokkan, K.A., Yamazaki, S., Tei, H., Sakaki, Y. & Menaker, M. Entrainment of the circadian clock in the liver by feeding. *Science* **291**, 490-493 (2001).
22. Damiola, F., *et al.* Restricted feeding uncouples circadian oscillators in peripheral tissues from the central pacemaker in the suprachiasmatic nucleus. *Genes Dev* **14**, 2950-2961 (2000).
23. Nakahata, Y., *et al.* The NAD⁺-dependent deacetylase SIRT1 modulates CLOCK-mediated chromatin remodeling and circadian control. *Cell* **134**, 329-340 (2008).
24. Asher, G., *et al.* SIRT1 regulates circadian clock gene expression through PER2 deacetylation. *Cell* **134**, 317-328 (2008).
25. Masri, S., *et al.* Partitioning circadian transcription by SIRT6 leads to segregated control of cellular metabolism. *Cell* **158**, 659-672 (2014).
26. Li, L., *et al.* SIRT7 is a histone desuccinylase that functionally links to chromatin compaction and genome stability. *Nat Commun* **7**, 12235 (2016).
27. Barber, M.F., *et al.* SIRT7 links H3K18 deacetylation to maintenance of oncogenic transformation. *Nature* **487**, 114-118 (2012).
28. Vazquez, B.N., *et al.* SIRT7 promotes genome integrity and modulates non-homologous end joining DNA repair. *EMBO J* **35**, 1488-1503 (2016).
29. Dubrovsky, Y.V., Samsa, W.E. & Kondratov, R.V. Deficiency of circadian protein CLOCK reduces lifespan and increases age-related cataract development in mice. *Aging (Albany NY)* **2**, 936-944 (2010).
30. Turek, F.W., *et al.* Obesity and metabolic syndrome in circadian Clock mutant mice. *Science* **308**, 1043-1045 (2005).
31. Kondratov, R.V., Kondratova, A.A., Gorbacheva, V.Y., Vykhovanets, O.V. & Antoch, M.P. Early aging and age-related pathologies in mice deficient in BMAL1, the core component of the circadian clock. *Genes Dev* **20**, 1868-1873 (2006).
32. Kornmann, B., Schaad, O., Bujard, H., Takahashi, J.S. & Schibler, U. System-driven and oscillator-dependent circadian transcription in mice with a conditionally active liver clock. *PLoS Biol* **5**, e34 (2007).
33. Koronowski, K.B., *et al.* Defining the Independence of the Liver Circadian Clock. *Cell* **177**, 1448-1462 e1414 (2019).
34. Saini, C., *et al.* Real-time recording of circadian liver gene expression in freely moving mice reveals the phase-setting behavior of hepatocyte clocks. *Genes Dev* **27**, 1526-1536 (2013).
35. Houtkooper, R.H., Pirinen, E. & Auwerx, J. Sirtuins as regulators of metabolism and healthspan. *Nat Rev Mol Cell Bio* **13**, 225-238 (2012).
36. Dibner, C., Schibler, U. & Albrecht, U. The mammalian circadian timing system: organization and coordination of central and peripheral clocks. *Annu Rev Physiol* **72**, 517-549 (2010).
37. Fischer, A.W., *et al.* Leptin Raises Defended Body Temperature without Activating Thermogenesis. *Cell reports* **14**, 1621-1631 (2016).
38. Mohawk, J.A., Green, C.B. & Takahashi, J.S. Central and peripheral circadian clocks in mammals. *Annu Rev Neurosci* **35**, 445-462 (2012).
39. Balchin, D., Hayer-Hartl, M. & Hartl, F.U. In vivo aspects of protein folding and quality control. *Science* **353**, aac4354 (2016).

40. Kiran, S., Anwar, T., Kiran, M. & Ramakrishna, G. Sirtuin 7 in cell proliferation, stress and disease: Rise of the Seventh Sirtuin! *Cell Signal* **27**, 673-682 (2015).
41. Li, H., *et al.* Regulation of NF-kappaB activity by competition between RelA acetylation and ubiquitination. *Oncogene* **31**, 611-623 (2012).
42. Hirano, A., *et al.* FBXL21 regulates oscillation of the circadian clock through ubiquitination and stabilization of cryptochromes. *Cell* **152**, 1106-1118 (2013).
43. Yoo, S.H., *et al.* Competing E3 ubiquitin ligases govern circadian periodicity by degradation of CRY in nucleus and cytoplasm. *Cell* **152**, 1091-1105 (2013).
44. Godinho, S.I., *et al.* The after-hours mutant reveals a role for Fbxl3 in determining mammalian circadian period. *Science* **316**, 897-900 (2007).
45. Lamia, K.A., *et al.* AMPK Regulates the Circadian Clock by Cryptochrome Phosphorylation and Degradation. *Science* **326**, 437-440 (2009).
46. Mukherji, A., Kobiita, A. & Chambon, P. Shifting the feeding of mice to the rest phase creates metabolic alterations, which, on their own, shift the peripheral circadian clocks by 12 hours. *P Natl Acad Sci USA* **112**, E6683-E6690 (2015).
47. Lamia, K.A., *et al.* Cryptochromes mediate rhythmic repression of the glucocorticoid receptor. *Nature* **480**, 552-556 (2011).
48. Zhang, E.E., *et al.* Cryptochrome mediates circadian regulation of cAMP signaling and hepatic gluconeogenesis. *Nat Med* **16**, 1152-1156 (2010).
49. Yoshizawa, T., *et al.* SIRT7 controls hepatic lipid metabolism by regulating the ubiquitin-proteasome pathway. *Cell Metab* **19**, 712-721 (2014).
50. Huard, J., *et al.* The Route of Administration Is a Major Determinant of the Transduction Efficiency of Rat-Tissues by Adenoviral Recombinants. *Gene Ther* **2**, 107-115 (1995).
51. Shaw, R.J., *et al.* The kinase LKB1 mediates glucose homeostasis in liver and therapeutic effects of metformin. *Science* **310**, 1642-1646 (2005).
52. Le Minh, N., Damiola, F., Tronche, F., Schutz, G. & Schibler, U. Glucocorticoid hormones inhibit food-induced phase-shifting of peripheral circadian oscillators. *EMBO J* **20**, 7128-7136 (2001).
53. Asher, G., *et al.* Poly(ADP-ribose) polymerase 1 participates in the phase entrainment of circadian clocks to feeding. *Cell* **142**, 943-953 (2010).
54. Vollmers, C., *et al.* Time of feeding and the intrinsic circadian clock drive rhythms in hepatic gene expression. *Proc Natl Acad Sci U S A* **106**, 21453-21458 (2009).
55. Mukherji, A., *et al.* Shifting eating to the circadian rest phase misaligns the peripheral clocks with the master SCN clock and leads to a metabolic syndrome. *Proc Natl Acad Sci U S A* **112**, E6691-6698 (2015).
56. Shi, G., *et al.* Dual roles of FBXL3 in the mammalian circadian feedback loops are important for period determination and robustness of the clock. *Proc Natl Acad Sci U S A* **110**, 4750-4755 (2013).
57. Siepka, S.M., *et al.* Circadian mutant Overtime reveals F-box protein FBXL3 regulation of cryptochrome and period gene expression. *Cell* **129**, 1011-1023 (2007).
58. Czarna, A., *et al.* Structures of Drosophila Cryptochrome and Mouse Cryptochrome1 Provide Insight into Circadian Function. *Cell* **153**, 1394-1405 (2013).
59. Tamanini, F., Chaves, I., Bajek, M.I. & van der Horst, G.T.J. Structure function analysis of mammalian cryptochromes. *Cold Spring Harb Sym* **72**, 133-139 (2007).

60. Khan, S.K., *et al.* Identification of a Novel Cryptochrome Differentiating Domain Required for Feedback Repression in Circadian Clock Function. *J Biol Chem* **287**, 25917-25926 (2012).
61. Chaves, I., *et al.* Functional evolution of the photolyase/cryptochrome protein family: Importance of the C terminus of mammalian CRY1 for circadian core oscillator performance. *Mol Cell Biol* **26**, 1743-1753 (2006).
62. Feillet, C.A., *et al.* Lack of food anticipation in Per2 mutant mice. *Curr Biol* **16**, 2016-2022 (2006).
63. Liu, S., *et al.* Involvement of the suprachiasmatic nucleus in body temperature modulation by food deprivation in rats. *Brain Res* **929**, 26-36 (2002).
64. Lopez, M., *et al.* Hypothalamic AMPK and fatty acid metabolism mediate thyroid regulation of energy balance. *Nat Med* **16**, 1001-1008 (2010).
65. Kim, K.W., *et al.* Steroidogenic factor 1 directs programs regulating diet-induced thermogenesis and leptin action in the ventral medial hypothalamic nucleus. *Proc Natl Acad Sci U S A* **108**, 10673-10678 (2011).
66. Orozco-Solis, R., *et al.* The Circadian Clock in the Ventromedial Hypothalamus Controls Cyclic Energy Expenditure. *Cell Metab* **23**, 467-478 (2016).
67. Martinez de Morentin, P.B., *et al.* Estradiol regulates brown adipose tissue thermogenesis via hypothalamic AMPK. *Cell Metab* **20**, 41-53 (2014).
68. Arble, D.M., Bass, J., Laposky, A.D., Vitaterna, M.H. & Turek, F.W. Circadian timing of food intake contributes to weight gain. *Obesity (Silver Spring)* **17**, 2100-2102 (2009).
69. Mukherji, A., Kobiita, A. & Chambon, P. Shifting the feeding of mice to the rest phase creates metabolic alterations, which, on their own, shift the peripheral circadian clocks by 12 hours. *Proc Natl Acad Sci U S A* **112**, E6683-6690 (2015).
70. Toledo, M., *et al.* Autophagy Regulates the Liver Clock and Glucose Metabolism by Degrading CRY1. *Cell Metab* **28**, 268-281 e264 (2018).
71. Chen, S.F., *et al.* Repression of RNA Polymerase I upon Stress Is Caused by Inhibition of RNA-Dependent Deacetylation of PAF53 by SIRT7. *Mol Cell* **52**, 303-313 (2013).
72. Ford, E., *et al.* Mammalian Sir2 homolog SIRT7 is an activator of RNA polymerase I transcription. *Gene Dev* **20**, 1075-1080 (2006).
73. Ryu, D., *et al.* A SIRT7-Dependent Acetylation Switch of GABP beta 1 Controls Mitochondrial Function. *Cell Metabolism* **20**, 856-869 (2014).
74. Fang, J., *et al.* Sirt7 promotes adipogenesis in the mouse by inhibiting autocatalytic activation of Sirt1. *Proc Natl Acad Sci U S A* **114**, E8352-E8361 (2017).
75. Gubin, D.G., Gubin, G.D., Waterhouse, J. & Weinert, D. The circadian body temperature rhythm in the elderly: effect of single daily melatonin dosing. *Chronobiol Int* **23**, 639-658 (2006).
76. Gubin, D.G., *et al.* Disrupted circadian rhythms of body temperature, heart rate and fasting blood glucose in prediabetes and type 2 diabetes mellitus. *Chronobiol Int* **34**, 1136-1148 (2017).
77. Yan, W.W., *et al.* Arginine methylation of SIRT7 couples glucose sensing with mitochondria biogenesis. *EMBO Rep* **19**(2018).
78. Liu, B., *et al.* Genomic instability in laminopathy-based premature aging. *Nat Med* **11**, 780-785 (2005).
79. Ran, F.A., *et al.* Genome engineering using the CRISPR-Cas9 system. *Nat Protoc* **8**, 2281-

2308 (2013).

Correspondence and requests for materials should be addressed to B.L.

Acknowledgements

This study was supported by grants from National Natural Science Foundation of China (81571374, 91849208, 81871114, 81601215), National Key R&D Program of China (2017YFA0503900), Science and Technology Program of Guangdong Province (2014A030308011, 2015A030308007, 2017B030301016), Shenzhen Municipal Commission of Science and Technology Innovation (JCYJ20160226191451487, KQJSCX20180328093403969, JCYJ20160520170240403, Discipline Construction Funding of Shenzhen 2016-1452). The authors are grateful to Dr. Jessica Tamanini (Shenzhen University and ETediting) for editing the manuscript prior to submission.

Author contributions

Z.L. and M.Q. planned the experiments under guidance of B.L., performed biochemical, cellular and *in vivo* experiments and analyzed data. X.T., S.Z., F.M., and X.C. generated cell lines and plasmids used in this study. W.H., S.S., G.L., C.X., J.S. and B.T. did *in vivo* experiments. B.L. designed and supervised this study. Z.L., M.Q., Q.P., B.Z., Z.W., Y.G., X.R. and B.L. prepared and revised the manuscript.

Competing interests

The authors declare no competing interests.

Figures

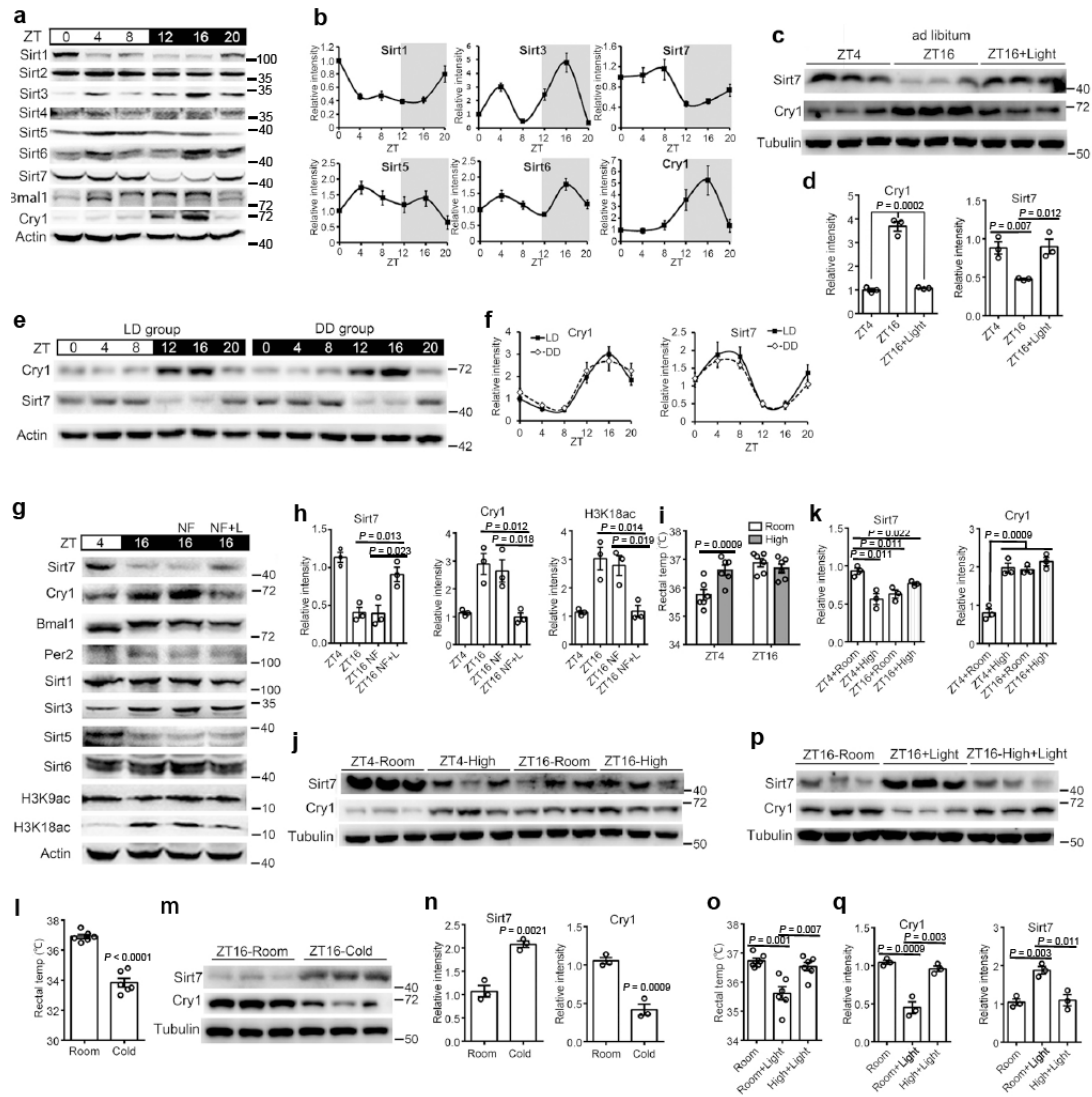


Figure 1. A light-entrained body temperature oscillation induces SIRT7 rhythmicity in the mouse liver.

(a) Representative immunoblots showing SIRT1-7 protein levels and indicated core clock factors in wild-type (WT) mouse liver across a circadian period. Liver tissues were collected at the indicated circadian times relative to Zeitgeber time (ZT). Representative immunoblots from three independent experiments are shown. n = 3 per time point. (b) Quantification of band intensities of three independent blots shown in (a). (c) Representative immunoblots showing SIRT7 and CRY1 protein levels in mouse livers, from mice maintained under normal feeding conditions with or without a 2-h light (L) pulse from ZT14 to ZT16. n = 3 per time point. (d) Quantification of band

intensities of three independent blots shown in (c), unpaired two-tailed Student's *t* test. (e) Representative immunoblots showing SIRT7 and CRY1 levels in the livers of mice maintained under 12:12 light/dark (LD) or dark/dark (DD) cycle. The DD group were placed in darkness for 24 h, and liver tissues were collected every 4 h for 24 h. *n* = 3 per time point. (f) Quantification of band intensities of three independent blots shown in (e). (g) Representative immunoblots showing the indicated protein levels under normal feeding or fasting (no food available from ZT0, NF) conditions with or without 2-h light exposure (L). Mice were fasted from ZT0 to ZT16 under a normal LD cycle or exposed to a 2-h light pulse from ZT14 to ZT16. *n* = 3 per time point. (h) Quantification of band intensities of three independent blots shown in (g), unpaired two-tailed Student's *t* test. (i) Mouse rectal temperature under room (R) or high (H) AT at ZT4 and ZT16. *n* = 6 per time point, unpaired two-tailed Student's *t* test. (j) Representative immunoblots showing SIRT7 and CRY1 protein levels under room temperature or high AT conditions at ZT4 and ZT16. *n* = 3 per time point. (k) Quantification of band intensities of three independent blots shown in (j), unpaired two-tailed Student's *t* test. (l) Mouse rectal temperature under room or cold (C) AT at ZT16. *n* = 6 per time point, unpaired two-tailed Student's *t* test. (m) Representative immunoblots showing protein levels of SIRT7 and CRY1 at ZT16 under room temperature or cold AT conditions at ZT16. *n* = 3 per time point. (n) Quantification of band intensities of three independent blots shown in (m), unpaired two-tailed Student's *t* test. (o) Mouse rectal temperature with 2-h light exposure under R or H AT at ZT16. *n* = 6 per time point, unpaired two-tailed Student's *t* test. (p) Representative immunoblots showing protein levels of SIRT7 and CRY1 in mouse liver with 2-h light exposure, when maintained at room temperature or at high AT conditions at ZT16. *n* = 3 per time point. (q) Quantification of band intensities of three independent blots shown in (p), unpaired two-tailed Student's *t* test. Data represent the means \pm s.e.m. of three independent experiments.

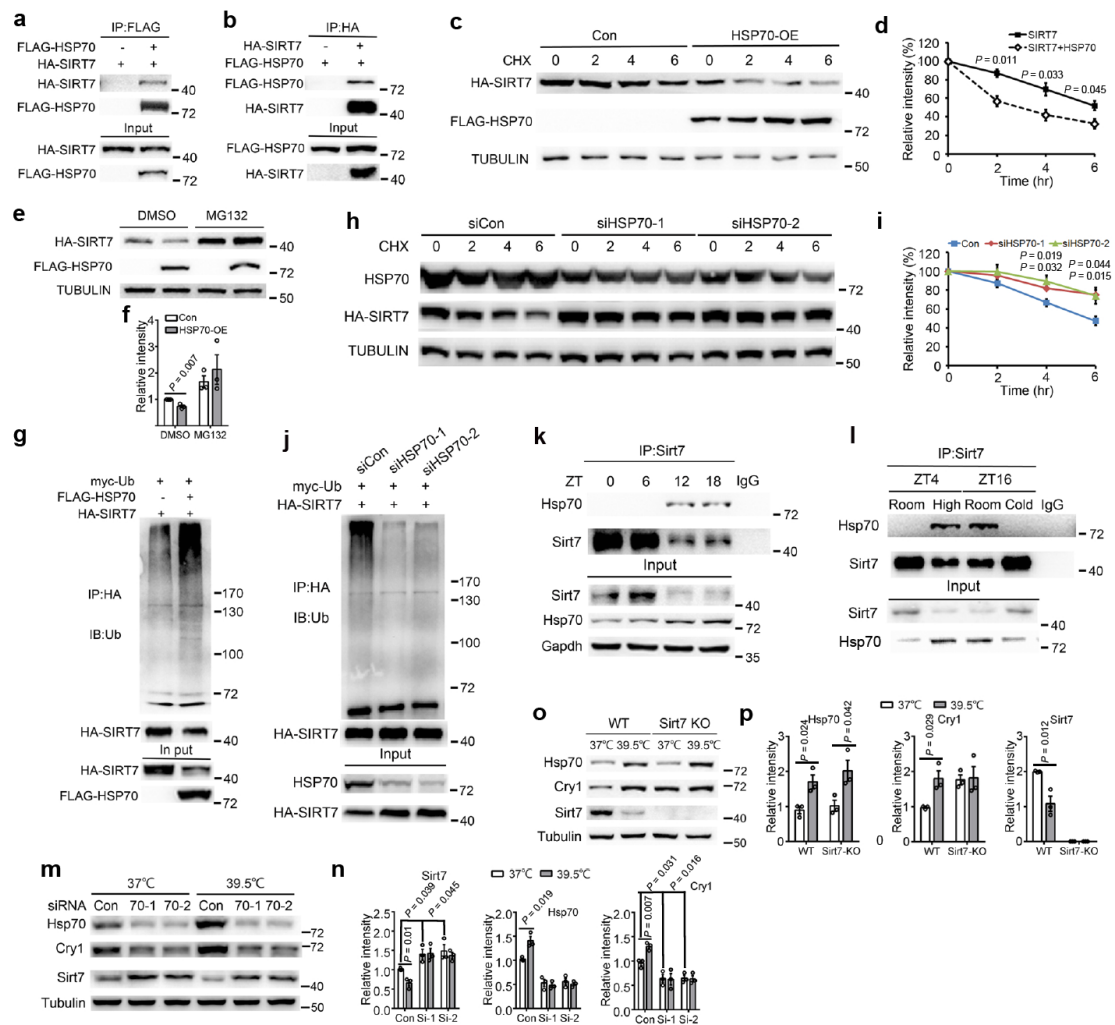


Figure 2. HSP70 mediates SIRT7 degradation via ubiquitin-proteasome pathway

(a,b) Co-immunoprecipitation (IP) was performed in HEK293 cells over-expressing HA-SIRT7 and FLAG-HSP70 (repeated three times with similar results). (c) Representative immunoblots showing SIRT7 levels in HEK293 cells expressing FLAG-HSP70 and HA-SIRT7 treated with 50 μ g/ml cycloheximide (CHX). (d) Quantification of SIRT7 protein levels in (c), unpaired two-tailed Student's *t* test. (e) Representative immunoblots showing SIRT7 levels in HEK293 cells expressing FLAG-HSP70 and HA-SIRT7 treated with 20 μ M MG132 for 6 h. (f) Quantification of SIRT7 protein levels in (e), unpaired two-tailed Student's *t* test. (g) Ubiquitination of SIRT7 in the absence or presence of FLAG-HSP70 in HEK293 cells (repeated three times with similar results). (h) Representative immunoblots showing SIRT7 levels in Scramble (siCon) or siHsp70-treated HEK293 cells in the presence of CHX (50 μ g/ml). (i) Quantification of SIRT7 protein levels in (h), unpaired two-tailed Student's *t* test. (j)

Ubiquitination of SIRT7 in Scramble or siHsp70-treated HEK293 cells (repeated three times with similar results). **(k)** The interaction between HSP70 and SIRT7 in mouse livers across a circadian cycle was examined by Co-IP (repeated three times with similar results). **(l)** The interaction between HSP70 and SIRT7 in mouse livers at various ATs was determined by Co-IP (repeated three times with similar results). **(m)** Representative immunoblots showing SIRT7, HSP70 and CRY1 protein levels in WT and *HSP70* KD MEFs with or without a 2-h heat shock at 39.5°C. **(n)** Quantification of SIRT7 protein levels in **(m)**, unpaired two-tailed Student's *t* test. **(o)** Representative immunoblots showing SIRT7, HSP70 and CRY1 protein levels in WT and *Sirt7*^{-/-} MEFs with or without 2-h heat shock at 39.5°C. **(p)** Quantification of SIRT7 protein levels in **(o)**, unpaired two-tailed Student's *t* test. Data represent the means \pm s.e.m. of three independent experiments.

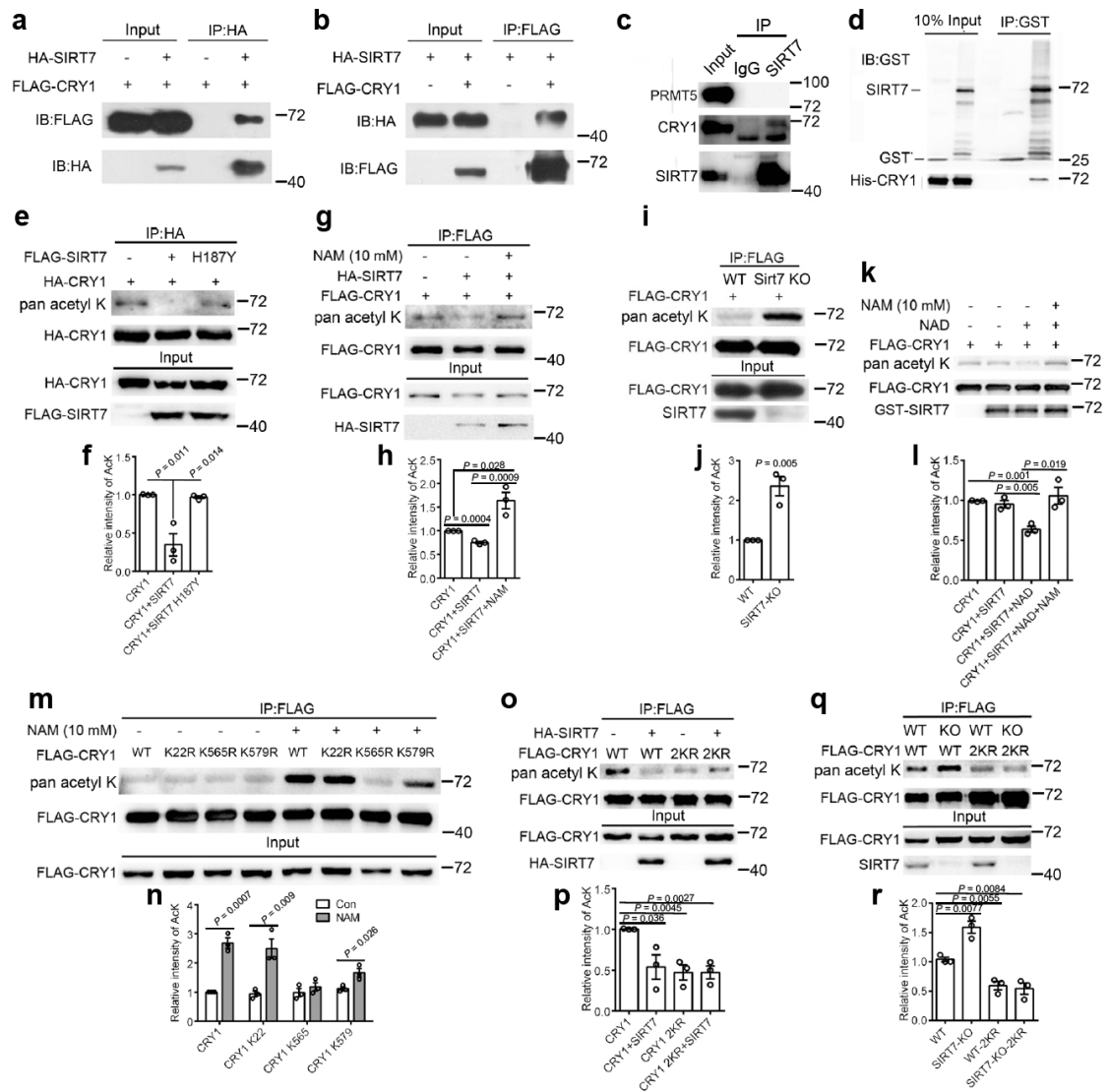


Figure 3. SIRT7 interacts with and deacetylates CRY1

(a,b) Co-immunoprecipitation (IP) was performed in HEK293 cells over-expressing HA-SIRT7 and FLAG-CRY1 (repeated three times with similar results). (c) The interaction between endogenous SIRT7 and CRY1 was determined by Co-IP in HEK293 cells. As negative control, an interaction between SIRT7 and PRMT5 was merely detected⁷⁷ (repeated three times with similar results). (d) GST pull-down assay showing a direct interaction between SIRT7 and CRY1 (repeated three times with similar results). (e) Acetylation level of CRY1 in the presence of SIRT7 or catalytically inactive SIRT7 H187Y mutant in HEK293 cells. (f) Quantification of acetylation of CRY1 in (e), unpaired two-tailed Student's *t* test. (g) Acetylation level of CRY1 in the presence of SIRT7 and/or 10 mM nicotinamide (NAM) in HEK293 cells. (h) Quantification of acetylation of CRY1 in (g), unpaired two-tailed Student's *t* test. (i)

Representative immunoblots showing FLAG-CRY1 acetylation in *SIRT7* KO HEK293 cells. **(j)** Quantification of acetylation of CRY1 in **(i)**, unpaired two-tailed Student's *t* test. **(k)** FLAG-CRY1 was immunoprecipitated and then incubated with purified GST-SIRT7, 1 mM NAD⁺ or 10 mM NAM. Acetylation of FLAG-CRY1 was detected with pan-acetyl K antibodies. **(l)** Quantification of acetylation of CRY1 in **(k)**, unpaired two-tailed Student's *t* test. **(m)** Representative immunoblots showing the acetylation levels of WT and FLAG-CRY1-KR in the absence or presence of 10 mM NAM in HEK293 cells. KR mutant constructs have lysine (K) residues K22, K565 and K579 mutated to arginine (R) by site-directed mutagenesis. **(n)** Quantification of acetylation of CRY1 in **(m)**, unpaired two-tailed Student's *t* test. **(o)** Acetylation level of FLAG-CRY1-2KR in HEK293 cells overexpressing HA-SIRT7. **(p)** Quantification of acetylation of CRY1 in **(o)**, unpaired two-tailed Student's *t* test. **(q)** Representative immunoblots showing acetylation levels of FLAG-CRY1-2KR in *SIRT7* KO HEK293 cells. **(r)** Quantification of acetylation of CRY1 in **(q)**, unpaired two-tailed Student's *t* test. Data represent the means \pm s.e.m. of three independent experiments.

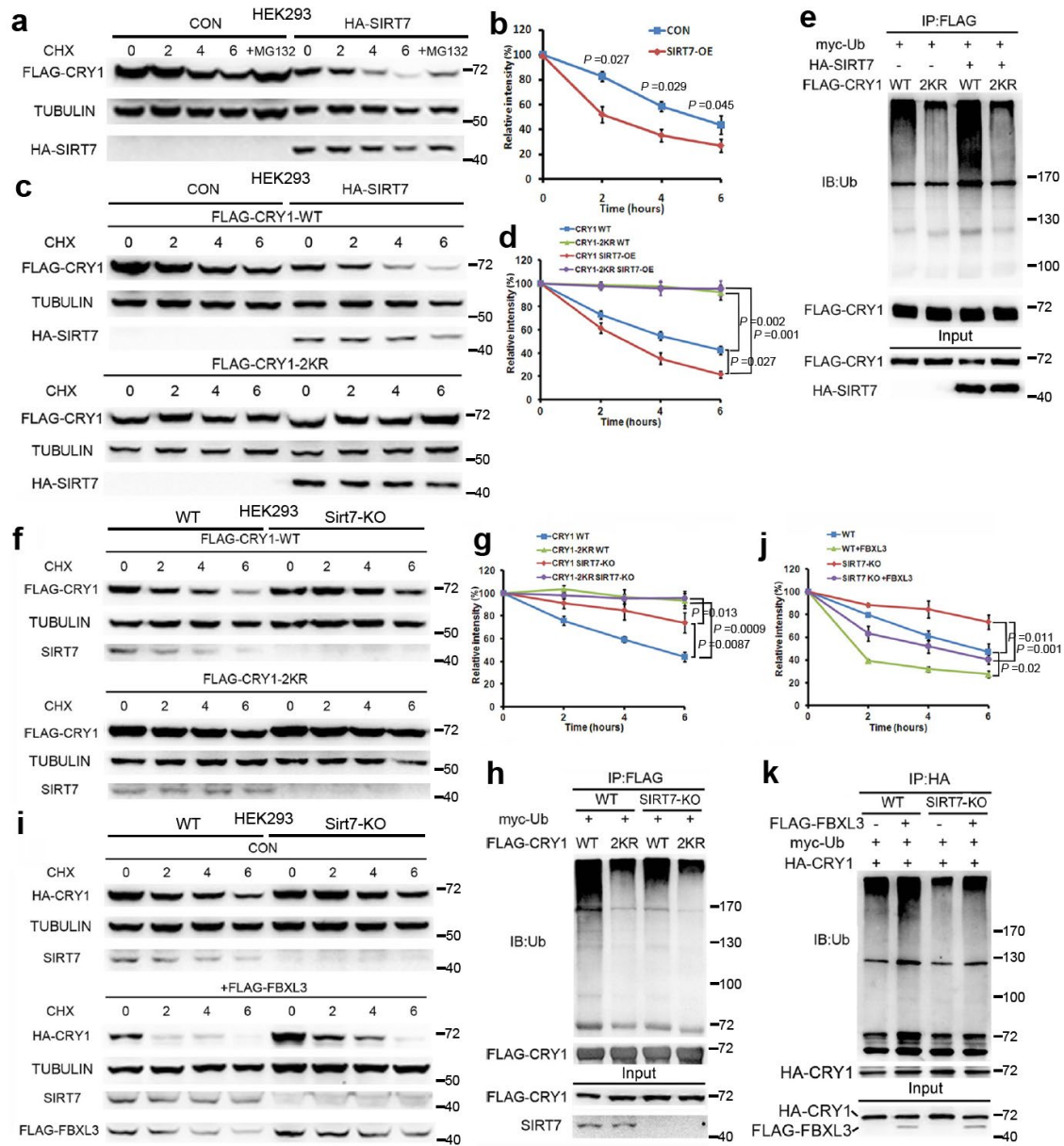


Figure 4. SIRT7-mediated deacetylation destabilizes CRY1

(a) Representative immunoblots showing CRY1 levels in HEK293 cells expressing FLAG-CRY1 alone (control, CON) or co-overexpressing FLAG-CRY1 and HA-SIRT7 and treated with 50 μ g/ml cycloheximide (CHX) and/or 20 μ M MG132. (b) Quantification of CRY1 protein degradation in (a), unpaired two-tailed Student's *t* test. (c) Representative immunoblots showing FLAG-CRY1 and FLAG-CRY1-2KR degradation in the presence or absence of HA-SIRT7 in HEK293 cells. KR mutant constructs have had lysine (K) residues mutated to arginine (R) by site-directed mutagenesis. (d) Quantification of CRY1 protein degradation in (c), unpaired two-tailed Student's *t* test. (e) Ubiquitination of CRY1 and CRY1-2KR in the absence or

presence of HA-SIRT7 in HEK293 cells (repeated three times with similar results). **(f)** Representative immunoblots showing the degradation rate of FLAG-CRY1 and FLAG-CRY1-2KR in *SIRT7* KO HEK293 cells that have been generated by CRISPR/Cas9 procedure. **(g)** Quantification of CRY1 protein degradation in **(f)**, unpaired two-tailed Student's *t* test. **(h)** Representative immunoblots showing ubiquitination (Ub) of FLAG-CRY1 and FLAG-CRY1-2KR in *SIRT7* KO HEK293 cells (repeated three times with similar results). **(i)** Representative immunoblots showing the effect of FBXL3 on CRY1 protein degradation in *SIRT7* KO HEK293 cells. **(j)** Quantification of CRY1 protein levels in **(i)**, unpaired two-tailed Student's *t* test. **(k)** Representative immunoblots showing FBXL3-mediated ubiquitination of FLAG-CRY1 in *SIRT7* KO HEK293 cells (repeated three times with similar results). Data represent the means \pm s.e.m. of three independent experiments. The statistics in **d**, **g** and **j** represent the comparison of protein intensity at time point 8.

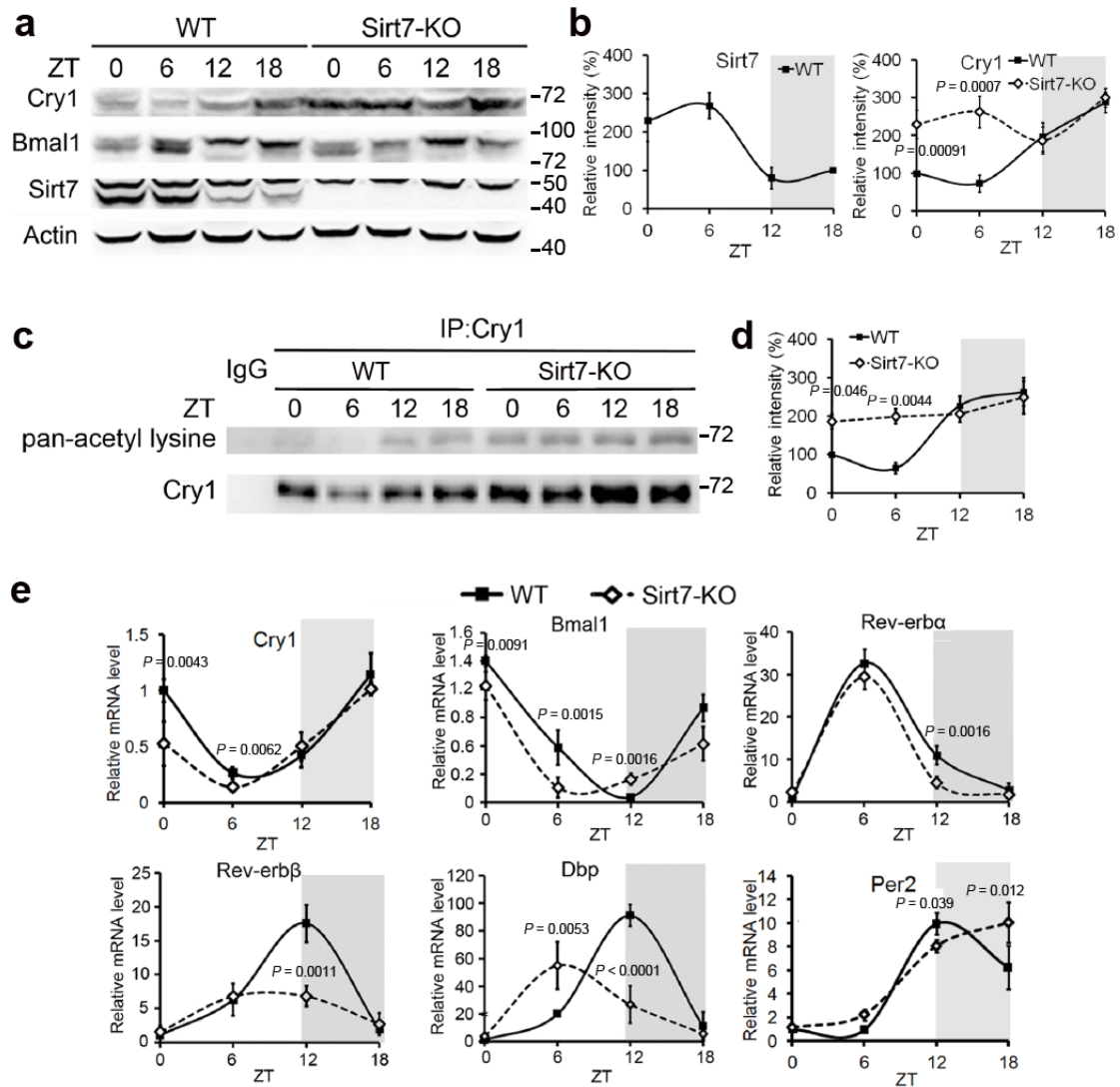


Figure 5. SIRT7 regulates the circadian phase in mouse livers.

(a) Core clock protein oscillations in WT and *Sirt7*^{-/-} liver tissues. Representative immunoblots are shown. n = 3 mice per genotype per time point. (b) Quantification of CRY1 and SIRT7 protein levels in (a). (c) Acetylation of CRY1 in WT (left) and *Sirt7*^{-/-} (right) mouse livers. Liver extracts from WT and *Sirt7*^{-/-} mice were immunoprecipitated with a CRY1 antibody. n = 3 mice per genotype per time point. (d) Quantification of CRY1 acetylation from three independent blots in (c). (e) Real-time PCR analysis of circadian clock genes in WT and *Sirt7*^{-/-} liver tissues isolated from *Sirt7*^{-/-} mice. n = 4 mice per genotype per time point. Data represent the means \pm s.e.m. of three independent experiments. Two-way ANOVA followed by Bonferroni's multiple comparisons test.

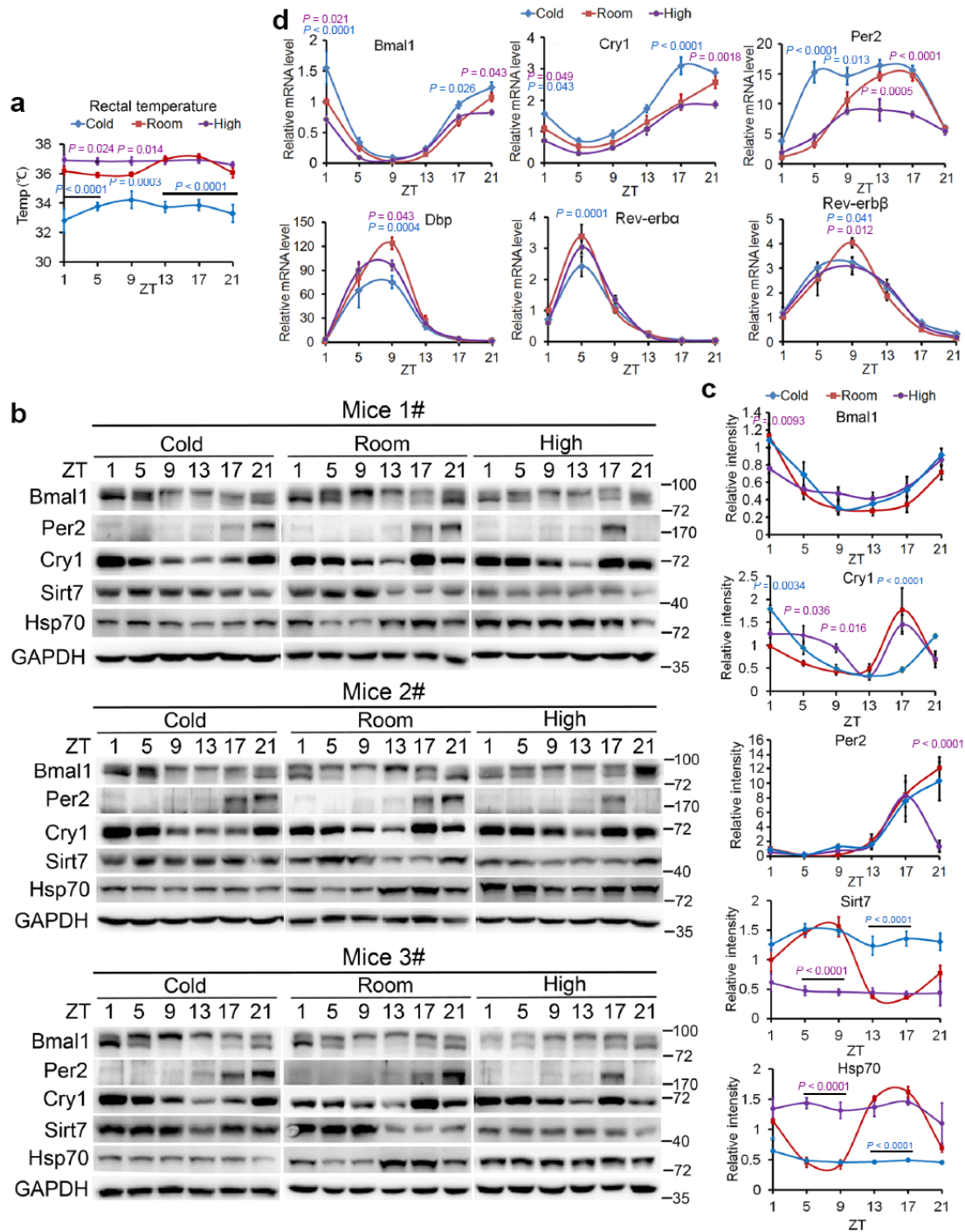


Figure 6. Expression of clock components at different ambient temperature conditions.

(a) Measurements of mouse rectal temperature by acute AT challenge. $n = 6$ mice per time point. (b) Representative immunoblots showing indicated protein levels at different AT. Mice were first housed at 22°C for 3 weeks. For temperature challenge, the mice were transferred to 4°C and 32°C conditions at ZT12. After 12-hr treatment,

liver samples were collected at indicated times $n = 3$ mice per time point. **(c)** Quantification of band intensity in **(b)**. **(d)** Real-time PCR analysis of mRNA levels of core clock genes at different AT. Data represent the means \pm s.e.m. of three independent experiments. Two-way ANOVA followed by Bonferroni's multiple comparisons test. Room: 22°C, High: 32°C, Cold: 4°C. **Purple P**, Room Vs High; **Blue P**, Room Vs Cold.

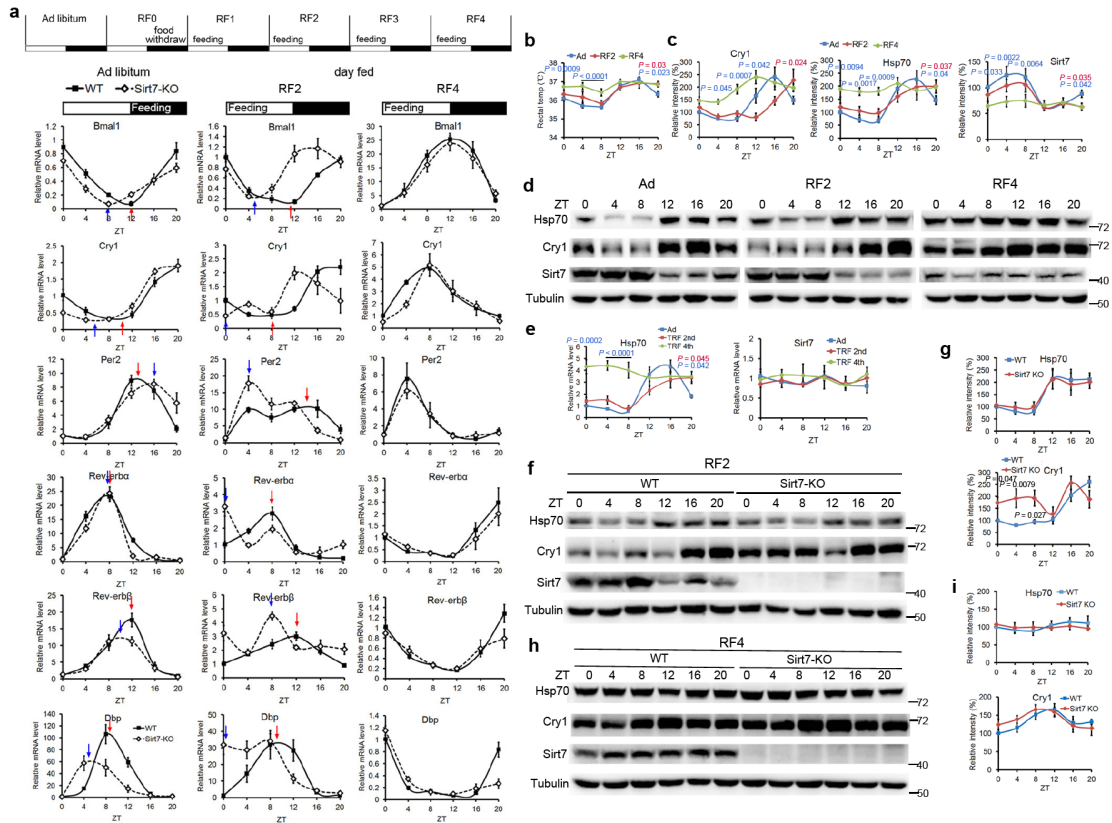


Figure 7. SIRT7 counteracts phase-shifting of hepatic clocks induced by restricted feeding.

(a) Real-time PCR analysis of mRNA levels of core clock genes in WT and *Sirt7*^{-/-} mice fed *ad libitum* or fed exclusively during daytime. n = 3 mice per genotype per time point. Arrows indicate the maximum or minimum expression levels of the respective genes in an examined circadian cycle. (b) Measurements of mouse rectal temperature during RF. n = 6 mice per time point. (c) Quantification of band intensities of three independent blots in (d). n = 3 mice per time point. (d) Representative immunoblots showing HSP70, SIRT7 and CRY1 protein levels in WT mice livers during RF. n = 3 mice per genotype per time point. (e) Real-time PCR analysis of *Hsp70* and *Sirt7* mRNA levels in WT mice fed *ad libitum* and during RF. n = 3 per time point. (f) Representative immunoblots showing HSP70, SIRT7 and CRY1 protein levels at RF2 in WT and *Sirt7*^{-/-} mice liver. n = 3 mice per genotype per time point. (g) Quantification of band intensities of three independent blots in (f). (h) Representative immunoblots showing HSP70, SIRT7 and CRY1 protein levels at RF4 in WT and *Sirt7*^{-/-} mice liver. (i) Quantification of band intensities in (h). Data represent the means \pm s.e.m. of three independent experiments, two-way ANOVA followed by Bonferroni's multiple

comparisons test. Blue *P*, Ad Vs RF4; Red *P*, Ad Vs RF2.

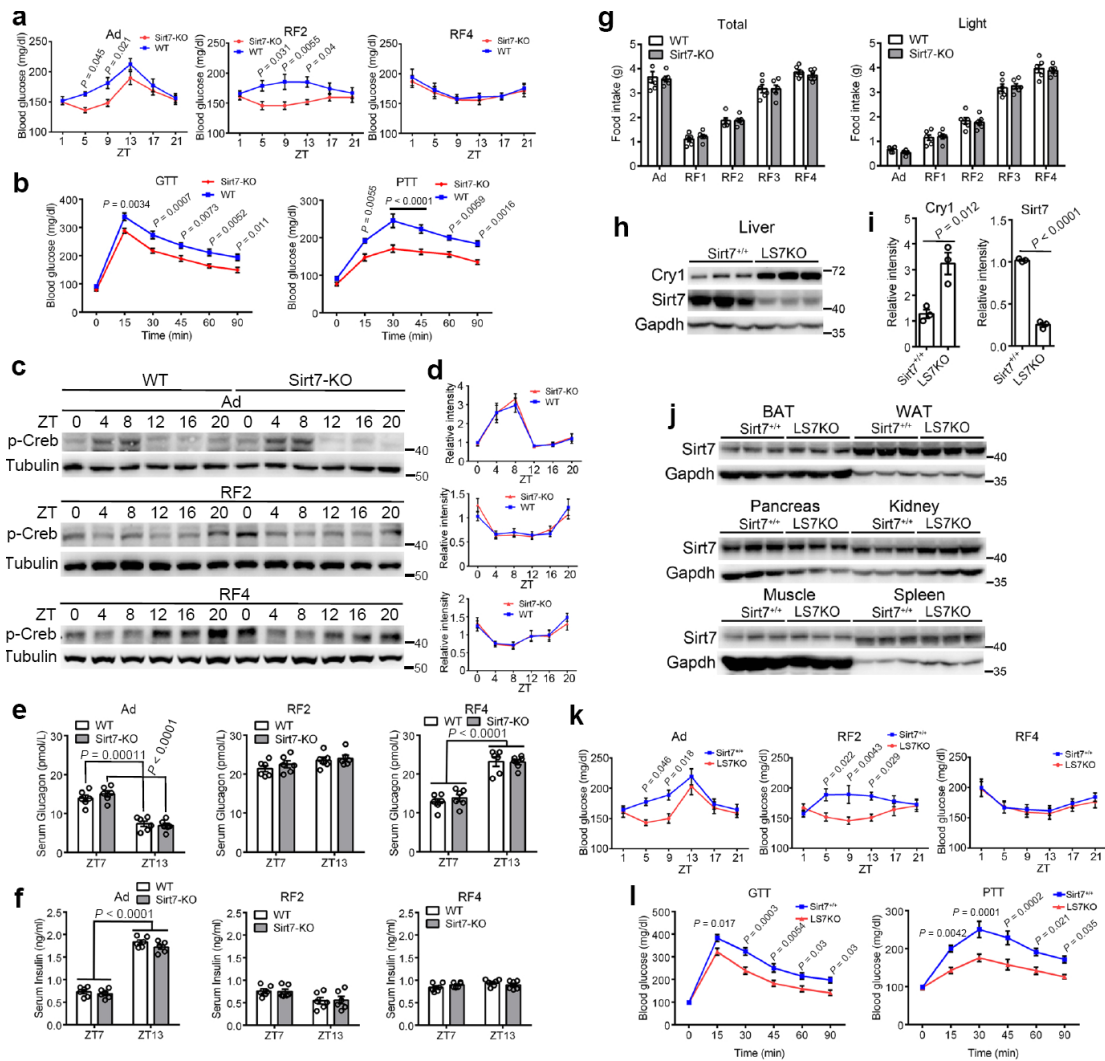


Figure 8. *Sirt7* deficiency leads to impaired hepatic gluconeogenesis

(a) Blood glucose levels in WT and *Sirt7*^{-/-} mice. n = 6 mice per genotype per time point. (b) The GTT and PTT results in WT and *Sirt7*^{-/-} mice. n = 6 mice per genotype per time point. (c) Representative immunoblots showing p-CREB in WT and *Sirt7*^{-/-} mice during Ad and RF. n = 3 mice per genotype per time point. (d) Quantification of band intensity of p-CREB in (c). (e) Serum glucagon levels in WT and *Sirt7*^{-/-} mice during RF. n = 6 mice per genotype per time point, unpaired two-tailed Student's *t* test. (f) Serum insulin levels in WT and *Sirt7*^{-/-} mice during RF. n = 6 mice per genotype per time point, unpaired two-tailed Student's *t* test. (g) Food intake in WT and *Sirt7*^{-/-} mice during RF. n = 6 mice per genotype per time point. (h) Representative immunoblots showing SIRT7 and CRY1 protein levels in *Sirt7*^{+/+} and *Sirt7*^{fl/fl} (LS7KO) mice livers 2 weeks after adenoviral Cre injection. n = 3 mice per genotype. (i) Quantification of band intensities in (h). (j) Representative immunoblots showing SIRT7 protein levels

in *Sirt7*^{+/+} and *LS7KO* mice tissues 2 weeks after adenoviral Cre injection. n = 3 mice per genotype. (k) Blood glucose levels in *Sirt7*^{+/+} and *LS7KO* mice. n = 6 mice per genotype per time point. (l) The GTT and PTT results in *Sirt7*^{+/+} and *LS7KO*. n = 6 mice per genotype per time point. Data represent the means \pm s.e.m. of three independent experiments. Student's *t* test or two-way ANOVA followed by Bonferroni's multiple comparisons test.

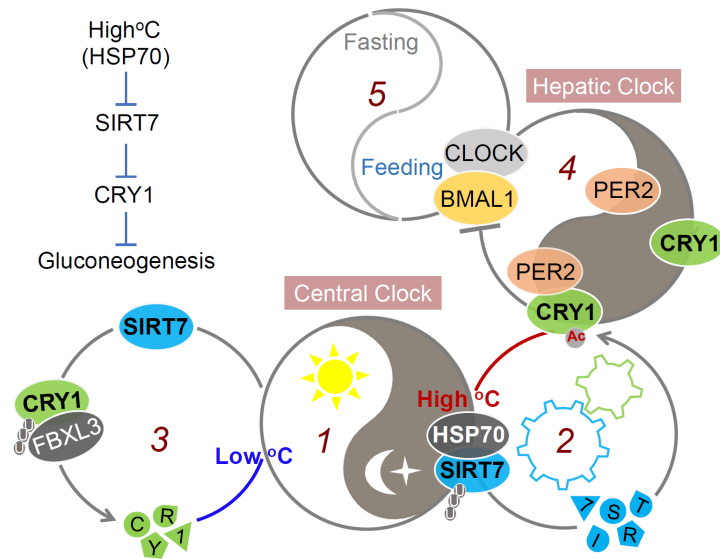


Figure 9. SIRT7 ensures phase coherence between the central and peripheral clocks and maintains glucose homeostasis.

A light-entrained BT cycle induces rhythmic HSP70 expression in the liver (*Cycle 1*). HSP70 interacts with SIRT7 and promotes proteasomal degradation (*Cycle 2*), thus synchronizing the hepatic clock. When at a high level, SIRT7 deacetylates CRY1 to promote FBXL3-mediated ubiquitination and subsequent degradation (*Cycle 3*), thus coupling the central pacemaker to the hepatic clock (*Cycle 4*). The BT/HSP70-SIRT7-CRY1 axis-mediated synchronization of hepatic clock is independent of FF cycle (*Cycle 5*), which rather counteracts the FF-entrained circadian phase in the liver. SIRT7 regulates gluconeogenesis via CRY1-mediated transcriptional suppression.